Contents

List of Figures

1 Introduction

Chaos is a multidisciplinary new science whose study by a large number of people is possible because of the personal computer. Almost no progress was possible before the advent of the PC because of the nonlinear equations that are necessary for chaos to occur. Nonlinearity does not of itself guarantee chaos; i.e., it is not sufficient, but it is necessary. For example, the "bell-ringer" mode of the planer rigid pendulum (Fig. 23, p. 33, 1st part) is a very nonlinear mode, but it is not chaotic. It's an example of a period-1 limit cycle. The single biggest problem concerning analytic treatment of nonlinear systems is probably the failure of superposition. Thus the powerful transform techniques so common to linear systems cannot be applied.

The dynamics of all cases treated in this monograph is what is called "deterministic chaos", a seeming oxymoron. Actually, the two words are not incompatible; since the original meaning of the Greek word, chaos, is not the same as is commonly employed today. The original meaning had to do with the state of the cosmos before order was established; i.e., the creative process. Inherent within the dynamics are richly organized patterns, reminiscent of living things.

Chaos implies unpredictability, but deterministic means that the source of the chaos is mathematically precise. For years, chaos was seen in various systems, both mechanical and electrical. No one was bold enough to recognize that the system itself was responsible for what masqueraded as noise. Instead it was incorrectly attributed to the environment. Unlike chaos, noise is devoid (because of randomness) of the richly organized structures that we now recognize as fractals.

It is now easy, with the personal computer, to study a large number of chaotic systems, both theoretically and experimentally. The software package, named TELAWARE, that is supplied with this monograph has a large number of algorithms with which one can (i) illustrate the difference between noise and chaos, and (ii) investigate a potpourri of chaotic systems, both experimentally and theoretically. Concerning the latter, the theoretical simulations number nearly 50, many of which are well known because of their historical significance (such as the Lorenz system and the Logistic map). Additionally, however, a number of recently discovered mechanical oscillators are treated in the General Simulations Menu (GSM). For more details of the physics concerning these, refer to the Peters Automated Pendula (PAPA) section of part I of this monograph.

The experimental investigations are presently limited to the Multipurpose Chaotic Pendulum (MPCP) sold by TEL-Atomic, Inc. The computer algorithms which are used with the MPCP are found in the Hardware Interface Menu (HIM), which is accessed by entering 'H' of the introductory menu. Embedded within HIM (accessed by entering 'P') is a Pendulum Simulations Menu (PSM); which contains 6 simulations of the conventional pendulum.

The total number of TELAWARE programs is currently 53, of which 5 require the MPCP; i.e., they cannot be executed unless the pendulum is physically connected. The menus with which the user "surfs" through TELAWARE are shown in Figures 1 through 4.

Some exercises which are possible with the PSM are described in part I of this document. The present part II is concerned primarily with simulations other than the pendulum. Of course, one may execute the pendulum programs without owning a multi-purpose chaotic pendulum.

```
                    MAIN SELECTION MENU
 ..........................................................
                        `TELAWARE'
 (Software to Computer Interface the Multipurpose Chaotic Pendulum
   and to perform Simulations related to Chaos and Complexity)

                        Tel Atomic, Inc
                       Jackson, Michigan
                         (800) 622-2866

                          Developed by:
                       Randall D. Peters, PhD

                        Physics Department
                       Texas Tech University
                          Lubbock, Texas
                          (806) 742-3757
 ..........................................................
              H -    Hardware Interfaces
                  (including Pendulum Simulations)
              S - General Software Simulations
              Q  -      Quit Program

                   Press your choice (`S', `H', or `Q')
```

Figure 1: The TELAWARE Introductory Menu.

```
  GENERAL SIMULATIONS MENU (Go to Hardware's `P' for conventional Pendulum)

01 - AUTOCORRELATION    15 - Logi. GRAPH. Const.   29 - STAIRCASE (DEVIL'S)
02 - BOUNCING BEAD      16 - LOGISTIC MAP          30 - SUPPORT CONSTR. PEND.
03 - BROWNIAN           17 - LORENZ RETURN MAP     31 - TIME'S ARROW
04 - BROWN. OSCILLATOR  18 - LORENZ TIME PLOT      32 - TORS. GRAV. P. (TGP)
05 - CHIRIKOV MAP       19 - LORENZ XY PLOT        33 - TGP1 for gen. FFT
06 - CIRCLE MAP         20 - LORENZ XZ PLOT        34 - TGP2 for gen. FFT
07 - DOUBLE PENDULUM    21 - LORENZ YZ PLOT        35 - TGP FOR FFT (Chaotic)
08 - DUFFING, TWO WELL  22 - LYAPUNOV EXP.(Logi.)  36 - TGP WITH BIG `b'
09 - ENTROPY, LOG. MAP  23 - PENDULUM EMULATOR     37 - THREE BODY, gravity
10 - HENON HEILE        24 - PETERS MAP            38 - TODA LATTICE WAVES
11 - HENON Map          25 - PROB. DISTR.          39 - VANDERPOL OSC.
12 - KAPITZA PENDULUM   26 - PWR. SPEC. (FFT)      40 - WAVE (simple)
13 - KDV SOLITON        27 - RETURN MAP, logi.     41 - WHITE NOISE & 1/f NOISE
14 - KRAZON             28 - SINE GORDON SOLITON   42 - ZANY ROOT FINDER

                    R - RETURN TO MAIN MENU
      (During operation, be sure Caps Lock and Num Lock are `off')

                    Enter Choice ( `1' - `42' or `R')
? _
```

Figure 2: The General Simulations Menu.

```
                    HARDWARE INTERFACE MENU

(WARNING: Unless Pendulum is connected, enter only `P' or `R')

              1 - Phase Space Plot
              2 - Position and Velocity vs Time
              3 - Poincare' Section
              4 - Drive Cycle Timing relative to Velocity
              5 - For FFT of Velocity, using #26, gen'l sim's.

              P - SIMULATIONS OF THE INTERFACED PENDULUM


              R - RETURN TO MAIN MENU


              Enter choice (`1' - `5', `P' or `R')
? _
```

Figure 3: The Hardware Interface Menu.

```
                 PENDULUM SIMULATIONS MENU


              1 - Phase Space Plot, standard
              2 - Phase Space Plot, Multipurpose Pendulum
              3 - Displacement (& velocity in blue) vs Time
              4 - Poincare' Section, standard
              5 - Poincare' Section, embedding th. based
              6 - Bellringer Mode (provides for FFT
                  of velocity using # 26, gen'l sim's menu)
              R - RETURN TO HARDWARE INTERFACE MENU
                 (Be sure Caps Lock & Num lock are `off')



              Enter choice (`1' - `6' or `R')
? _
```

Figure 4: The Pendulum Simulations Menu.

2 Noise

As with all of experimental physics, noise is part of the measurement process, being more important in some studies of chaos than others. It's important that one understand the difference between noise and chaos. Noise is external to the system being studied, and thus environmental; whereas chaos is intrinsic to the system. For years the chaotic dynamics of several systems were incorrectly thought to be noise.

There are four programs dealing with noise in the GENERAL SIMULATIONS MENU (GSM). They are: #3—a classical example of Brownian motion, #4—an oscillator that is Brownian motion excited, #31—the Arrow of Time, and #41—a generator of white noise or 1/f noise according to user selection.

The most important of all, 1/f noise, is one that cannot always be separated from experimental studies of chaos and complexity. This noise has been known for more than 50 years but it is still not well understood. It appears that one of the better candidates for explaining it is that due to Bak et al, known as self organized criticality (SOC). The mechanisms responsible for the necessary many body cooperation are not known, however. Furthermore, it should be noted that some experts in complexity do not believe in SOC.

It has been common to think in terms of a "generic" noise—that which is called "white", because it is very easy to produce white noise with the computer. This overly idealized approximation cannot be physically meaningful, except in a very narrow frequency range. Because of the contrasts between noise and deterministic chaos, and because noise is infrequently discussed in physics (not to mention erroneously treated); this package also contains some algorithms dealing with noise.

2.1 White noise

White noise (having no frequency dependence) is very easy to generate with the computer, using the Basic function, RND. This function generates variates that are governed by a uniform distribution. It is recommended that one look at both the temporal and spectral features of this, and indeed, all the noise cases of TELAWARE. One of the two output possibilities from GSM program #41 is shown in Fig. 5. Observe, in particular, that the power spectrum (mean value) is essentially flat for this white noise case. *Note: For this and all power spectra of this monograph the frequency plots terminate at 1/2 the Nyquist frequency.*

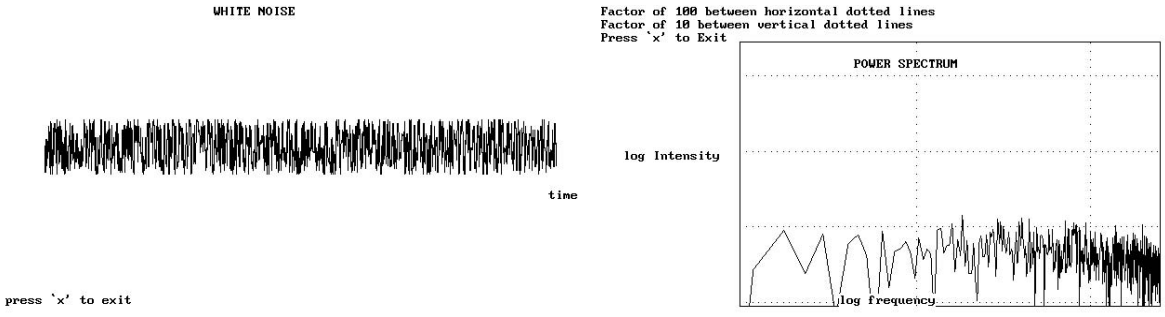

Figure 5: White noise.

(a). Time dependence (b). Frequency dependence (log-log plot)

The power spectrum is defined, for present purposes, as the sum of the squares of the real and imaginary parts of the Fourier transform of the temporal record. As mentioned in part I of this monograph, the transform is done via the Cooley-Tukey (fast Fourier transform, or FFT) algorithm. In Fig. 5, as in

all power spectra of this document, the separation between the horizontal dotted lines is a factor of 100. The abscissa may be linear or logarithmic according to user selection. In the latter case, the separation between vertical dotted lines is a factor of 10.

2.2 1/f Noise

Pink, or 1/f noise is more difficult to generate with the computer. Moreover, there are not many references to be found on the subject. Insofar as generating variates for a given distribution (in general), the various books written by D. Knuth are good references. A warning is in order! It is commonplace to do monte carlo processing in which the variates obey Gaussian statistics. Of course this distribution is not appropriate for positive definite quantities, if the variance is large enough to allow negative values (a case that actually happened on the U. S. antisatellite program in early studies of the miniature vehicle).

The pink noise generator used here is the one described by Sprott in the manual of his "Chaos Demonstrations", Physics Academic Software (1992), ISBN 0-88318-968-2, available from The Academic Software Library, Box 8202, North Carolina State University, Raleigh, NC 27695-8202. For the one who would like to program his own computer, since the AIP package does not have source code; Sprott's description of a pink noise algorithm was used to write the following program.

Due to the burgeoning nature of this document, the source code for all of the TELAWARE programs has not been explicitly included. Anyone desiring specific information on these programs (source code) should contact TEL-Atomic.

```
REM Basic program to generate (w)hite or (p)ink noise.
DIM u(5), ta(5), tn(5)
CLS
KEY 15, CHR$(0) + CHR$(&H2D)
ON KEY(15) GOSUB terminate
KEY(15) ON
OPEN "trial.dat" FOR OUTPUT AS #1
SCREEN 9
COLOR 15, 4
CLS
VIEW (50, 0)-(600, 300): WINDOW (-0!, -.4)-(.4, .4)
dt = .0002
j = 0
PRINT "input noise type--'(W)'hite, or '(P)'ink = 1/f"
INPUT sp$
CLS
LOCATE 23, 2: PRINT "press 'x' to exit"
IF sp$ = "p" THEN LOCATE 1, 30: PRINT "PINK NOISE"
IF sp$ = "w" THEN LOCATE 1, 30: PRINT "WHITE NOISE"
LOCATE 15, 75: PRINT "time"
jm = 4
start:
t = t + dt
k = k + 1
IF k = 4096 THEN CLOSE #2
IF k > 4096 THEN GOTO terminate
WRITE #1, 1 * u0n
u0 = INT(2 * 2 ^ jm * RND(1))
IF sp$ = "w" THEN GOTO 88
FOR j = 1 TO jm
ta(j) = INT(u0 / 2 ^ j)
IF ta(j) <> u0 / 2 ^ j THEN ta(j) = 0
IF ta(j) <> 0 THEN ta(j) = 1
```

```
NEXT j
GOTO 89
88 FOR j = 1 TO jm + 1
ta(j) = 2 ^ (j - 1) AND u0
IF ta(j) <> 0 THEN ta(j) = 1
NEXT j
89
u00 = RND(1): IF u00 < .5 THEN u00 = 0 ELSE u00 = 1
FOR jj = 1 TO jm
u(jj) = RND(1): IF u(jj) < .5 THEN u(jj) = 0 ELSE u(jj) = 1
IF ta(jj) = 1 THEN tn(jj) = u(jj)
NEXT jj
u0n = u00
FOR jl = 1 TO jm
u0n = u0n + 2 ^ jl * tn(jl) - 2 ^ (jm - 1) / 2
NEXT jl
LINE (tp, .005 * u0np)-(t, .005 * u0n)
PSET (t, 0)
tp = t
u0np = u0n
GOTO start
terminate:
END
```

The approximate method used is the following (quoting Sprott): "Start with an arbitrary five-bit binary number (which can have a decimal value between 0 and 31). Generate the next number in the series by randomly changing the bits of the current number in a way such that each bit is changed only half as often as the bit to its right. To do this, generate a random integer in the range 0 to 31. This integer will be divisible by one every time, by two half the time, by four one-quarter of the time etc. Thus, the integer can be used to decide which bits of the current number are eligible for change."

Shown in Fig. 6a is the output from GSM program #41 (code above, extracted from TELAWARE), after selecting 1/f noise. The power spectrum according to the 6a record is shown in Fig. 6b. The mean value of the noise (ignoring the lowest frequency section) should fall off as 1/f in a log-log plot—the basis for the nomenclature. It can be seen from the figure that the decline is really a little faster than 1/f, which speaks to the difficulty of building a true pink noise generator.

Pink noise is the most common noise type in the cosmos, showing up virtually everywhere. In addition to electronics cases which abound, it is even found in the mesodynamic world of mechanical oscillators (the interested reader may refer to references in the appendix thus labeled in part I of this document). In this case, evidently the atoms are playing "musical chairs"; which is necessary for anelasticity and (on a larger scale) creep. After half a century of noting its presence, pink noise is still poorly (if at all) understood.

In comparing figures 5 and 6, it can be readily seen that white noise has more high frequencies in it (the probability of significant amplitude jumps at any point in time is quite high). This shows up readily in the autocorrelation, as illustrated in Fig. 7; where the contrast between white (on the left) and pink (on the right) is marked.

2.3 Brownian motion

In the present work, Brownian noise is addressed by way of a particle moving under the influence of a fluctuating force. The dynamics of the particle is described by the Langevin equation [c.f. F. Reif, *Fundamentals of Statistical and Thermal Physics*, p. 560, McGraw Hill, New York (1965)]. It can be shown that the fluctuating force is intimately related to the dissipation (through the fluctuation-dissipation theorem). The equation of motion of the particle is given by

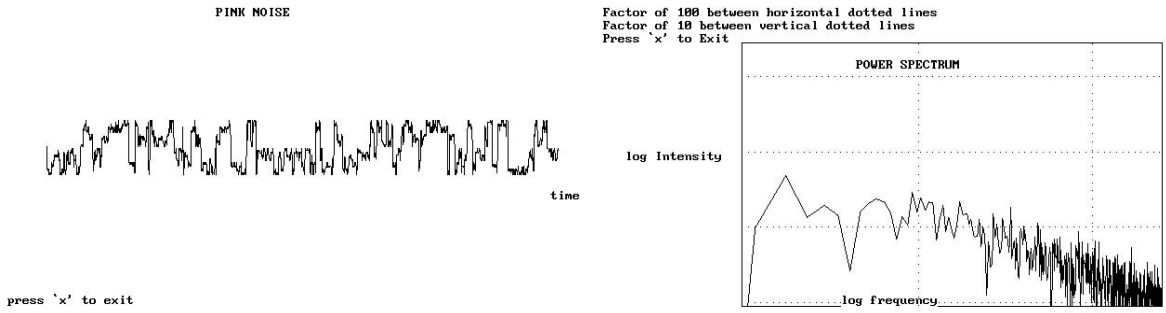

Figure 6: Approximate 1/f (= pink) noise.

(a). Time dependence. (b). Frequency dependence (log-log plot).

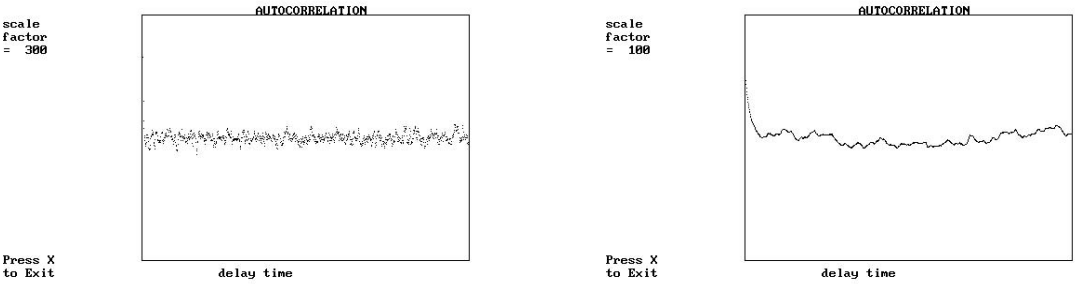

Figure 7: Autocorrelation of white noise (left) and pink noise (right).

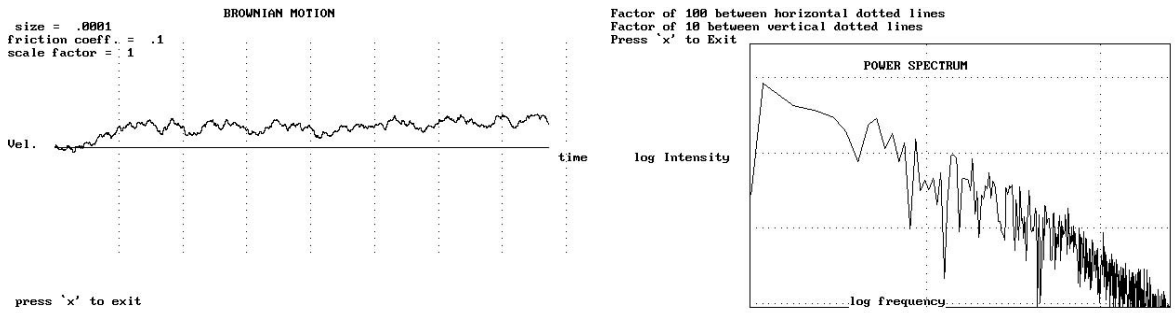

Figure 8: Brownian noise.

(a). Time dependence. (b). Frequency dependence (log-log plot).

$$m\frac{dv}{dt} \;=\; -\,\alpha v \;+\; F' \;+\; \mathcal{F} \tag{1}$$

where $\mathcal{F}$ is the external force on the particle, and F' is the rapidly fluctuating (environmental) part whose average value vanishes. Notice that in all of these noise treatments, the fluctuating part is external to the system (thus environmental), whereas chaos is internal.

In GSM program #3, it is the velocity of the particle that is plotted. (The displacement tends to drift off screen.) The fluctuating force, F', is generated using the RND function. One can show that the velocity noise is proportional to $1/f^2$ in the log-log power spectral plot, as shown on the right in Fig. 8. The temporal record that generated it is shown on the left. Note that a factor of 10 increase in the frequency is met with a factor of 100 decrease in spectral intensity.

Further observe that the falloff of the noise with frequency, in the log-log plot is definitely more rapid than the pink noise case.

Concerning Brownian motion, Present points out in his classic textbook [*Kinetic theory of Gases*, McGraw Hill, N.Y., (1958), p. 157] that there are two ways that Brownian motion can be seen: either by (i) reducing the number of molecules in the collection or by (ii) adopting more sensitive experimental methods, to detect and measure statistical fluctuations and to account theoretically for the observed results. The physics behind these statements is the following (quoting Present): "...the smaller the collection, or sample, to which statistical methods are applied, the larger are the percentage deviations from the average, or most probable, behavior. ..... with statistical fluctuations, it is shown that the root-mean-square relative fluctuation varies inversely with the square root of the size of the collection. The large numbers of molecules involved in all the gaseous phenomena that we have considered ensure that the statistical fluctuations are ordinarily imperceptible."

It is the second method (more sensitive experimental methods) that has permitted us to study Brownian motion with an SDC based pendulum. In particular, as part of the Physics 3204 (intermediate laboratory) at Texas Tech, we have been looking at a variety of pendulum interactions with air. Few realize, for example, that the damping of a pendulum does not fall off rapidly with pressure, until the pressure is such that the mean free path is comparable to chamber dimensions. The reason has to do with momentum transport. Present explains this in his treatment of viscosity according to the kinetic theory. Quoting from p. 38: "Viscosity in a gas originates, therefore, in the molecular transport of the momentum of flow in the direction of the velocity gradient (but opposite in sense)." He gives the following analogy: Imagine two trains on parallel adjacent tracks. "As the faster train overtakes and passes the slower one, packages are thrown across from each train to the other. The effect is to accelerate the slower train and decelerate the faster one." Interestingly, J. C. Maxwell was the first to consider

this problem. He deduced, from kinetic theory that he developed, that a pendulum swinging in vacuum should not experience any change in the log decrement. The students in Phys. 3204 have shown this to be approximately true until the gas becomes "ballistic"; i.e., the mean free path is greater than the chamber size.

2.4 Arrow of Time

In GSM program #4, the oscillator driven by Brownian motion is treated in the following way. As was noted (Present's theoretical statement), the fluctuation should vary inversely with the square root of the size. This is approximately true for the fluctuations encountered in the "Arrow of Time", GSM program #31. This program is a fascinating one which was first published by Eisberg [*Applied Mathematical Physics with Programmable Pocket Calculators*, McGraw Hill (1976), p. 129.] Eisberg was concerned with the 2nd law of thermodynamics (entropy). The system is a box with two chambers, divided by a partition through which only one molecule at a time can pass. The behaviour of the system can be simulated as follows, quoting Eisberg: "(1) generate a random number from 0 to 1; (2) test it against the current value of the fraction of molecules on the left; and (3) "move" a molecule from left to right if the number is smaller than the fraction, or in the opposite direction if it is larger, by subtracting or adding 1 to the appropriate storage registers. The results of this simulation will lead you to an understanding of why there is an irrevocable tendency for the disorder, or entropy, of the system to increase as time evolves, providing it contains a reasonably large number of molecules." The code which does this is as follows.

```
KEY 15, CHR$(0) + CHR$(&H2D)
ON KEY(15) GOSUB terminate
KEY(15) ON
RepeatArrow1:

    REM simulates the "arrow of time". Fluctuations large for small n
    REM Shift F5 to execute, Ctrl Break to stop, "r" to rerun with new n
    COLOR 7, 1
    CLS
    LOCATE 10, 10
    PRINT "input no. of particles (300 to 3000 is a good range)"
    INPUT n
    CLS
    nl = n: nr = 0: i = 0
    SCREEN 9
    COLOR 15, 4
    LOCATE 2, 35: PRINT "TIME'S ARROW"
    LOCATE 3, 30: PRINT "Number of particles ="; n
    LOCATE 2, 1: PRINT "All particles right"
    LOCATE 23, 1: PRINT "All particles left"

RepeatArrow2:
    i = i + 1
    u = RND(1)
    IF u < nl / n THEN nl = nl - 1
    IF u > nl / n THEN nl = nl + 1
    nr = n - nl
    PSET (.1 * i, nl * 345 / n), 3
    PSET (.1 * i, 2): PSET (.1 * i, 345)
    IF i = 7000 THEN GOTO donearrow
GOTO RepeatArrow2
donearrow:
```

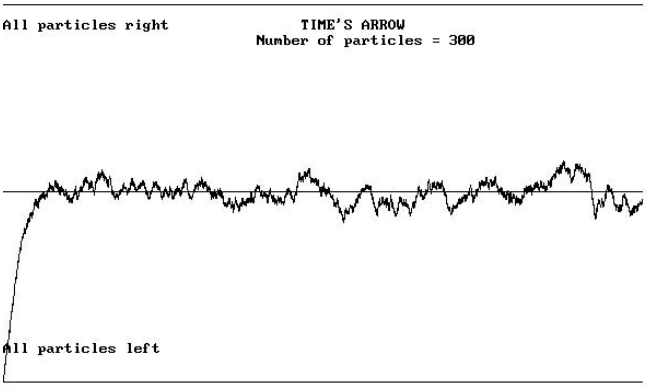

Figure 9: Illustration of the "Arrow of Time" (particle number is 300).

```
END
terminate:
END
```

Notice that the function RND is used. It provides variates in the range from 0 to 1 that are governed by a uniform (constant) distribution. For invertible functions, it is easy to use RND to obtain variates that are governed by a different distribution. For example, Log(RND) yields an exponential distribution. There are a variety of clever tricks to get things like the Gaussian (or when normalized, "normal") distribution. The best references to these important computational tools are the books written by D. Knuth.

For two reasons, the Arrow of Time program has been included within this monograph. One, it illustrates the 2nd law of thermodynamics; which says that the entropy of a real system (irreversible) can only increase. Interestingly, the equations of mechanics, based on calculus do not account for this. Time can run either direction and the equations don't care. Eventually, physics involving complexity will have to do a better job of dealing with this aspect of the real world. Along with a mathematician group, Tom Erber has thought about some of these things in relationship to the PLC effect. They have applied the concept of the "sneaky function", since the PLC effect violates the fundamental theorem of calculus (the functions and their derivatives are not continuous).

The second reason for considering the program has to do with its structure—it is a Monte Carlo based algorithm. Most real world systems of applied physics interest are too complex for first principles analytic treatment. For them, Monte Carlo methods are the only hope for meaningful simulation at this time. On a related note, we'll see that the generation of the Henon map requires first the filling of an x,y space by using random numbers. Thus the essence of the Monte Carlo method is used in a classical map of chaos (Henon was one of the first to produce a chaotic map, one showing fractal self similarity).

As shown in statistical mechanics (c.f. Reif , *Statistical and Thermal Physics*, McGraw Hill, 1965) the size of the fluctuations is proportional to $\frac{1}{\sqrt{n}}$. All of these features can be easily demonstrated with the program using different values of n. Fig. 9 is an example with n = 300.

The code just indicated was used to provide the drive of a simple harmonic oscillator in GSM program #4. An example output is given in Fig. 10. What is immediately evident in this figure (time plot), is that there are sustained periods of correlated motion. This also shows up as a well defined line in the power spectrum (Fig. 11a), and it is unmistakeable in the autocorrelation (Fig. 11b). There can be significant differences (particularly in the power spectrum) according to the size ("mass") of the oscillator.

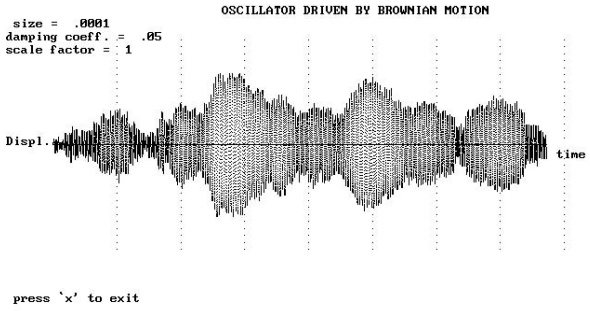

Figure 10: Motion of a Brownian driven simple harmonic oscillator.

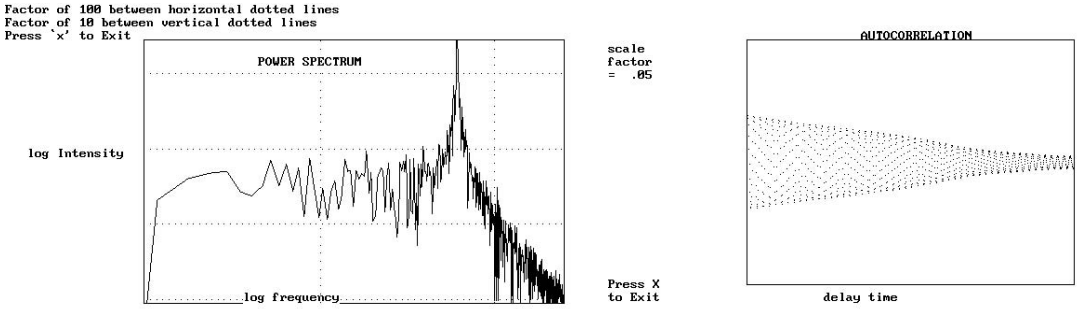

Figure 11: Power spectrum (left) and autocorrelation (right) corresponding to Fig. 10.

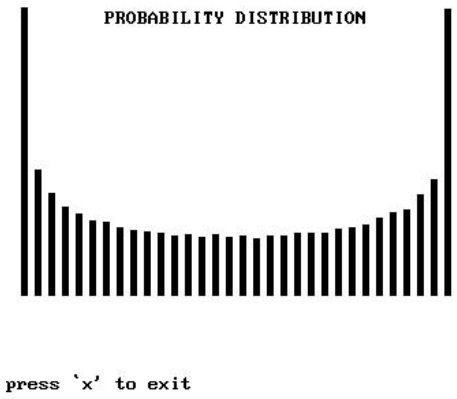

Figure 12: Probability distribution for low level periodic pendulum motion.

3 Probability Distribution

A tool that can be useful for assessing whether a data set is periodic, chaotic, or noisy is the probability distribution of the set. This technique is illustrated here in the beginning by considering the distribution of $x = cos\ \theta$, where θ is distributed uniformly over the interval, $-\pi < \theta < \pi$. The probability that θ is located between θ and $\theta + d\theta$ is given by

$$P(\theta)\ d\theta = \frac{d\theta}{2\pi} \tag{2}$$

The probability $Q(x)\ dx$ that $x = cos\ \theta$ is located between x and $x + dx$ is given by

$$Q(x)\ dx = 2\ P(\theta)\ d\theta \tag{3}$$

$$= 2\ P(\theta)\ dx/|\tfrac{dx}{d\theta}| \tag{4}$$

$$= \tfrac{dx}{\pi|sin\theta|} \tag{5}$$

(The reason for the factor of 2 is that there are two θ values corresponding to each value of x .) Thus the probability density is given by

$$Q(x) = \frac{1}{\pi\sqrt{1 - x^2}}\ ,\ -1 < x < 1\ ,\ 0 \text{ otherwise} \tag{6}$$

The "ears" on the distribution at the end points of a plot of Eq. (6) is characteristic of periodic motion. To show this, go to the pendulum simulations menu bell-ringer algorithm and execute with a drive frequency of 1.3. After the transients settle, the steady state (low level periodic) motion is written to memory (2048) values. Now return to the general simulations menu and run program #26. You'll obtain Fig. 12, showing these "ears".

To illustrate the difference between this periodic and other interesting cases, one may repeat the procedure using different algorithms. For example, Fig. 13 on the left corresponds to the chaotic TGP (GSM #35); and the right part of the same figure corresponds to white noise, generated with GSM #41. Similarly in Fig. 14, left and right respectively correspond to GSM #33 (periodic Duffing) and GSM #4 (Brownian oscillator).

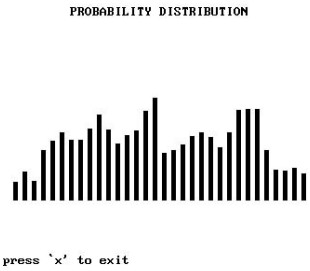

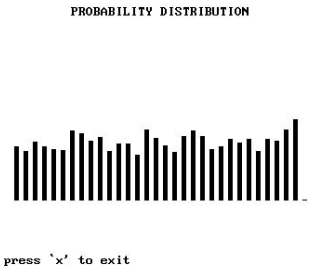

Figure 13: Probability Distributions.

(a). Chaotic case (b). White Noise

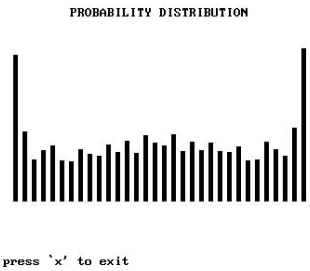

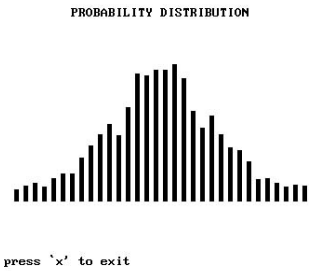

Figure 14: Probability Distributions.

(a). Periodic Duffing oscillator (b). Brownian oscillator

4 Traditional Chaos

There is no universally accepted criterion for saying that a system is chaotic or not. Usually the simultaneous satisfying of several criteria is considered necessary before the claim can be made with confidence. Among these criteria are: (i) nature of Poincare sections, (ii) nature of the power spectrum, (iii) algebraic sign of Lyapunov exponents, (iv) dimensionality, and (v) entropy. The existence of a positive Lyapunov exponent is probably the singlemost important test; however, it's calculation is not simple except with trivial systems. When an exponent is positive it means that two closely spaced trajectories in phase space diverge exponentially with time. Since the space is closed there must be "folding and stretching" like the making of taffy candy. This in turn gives rise to fractional dimensions (fractals in the terminology originated by Mandelbrot). If the phase space trajectories are followed indefinitely (time exposure), there is a dramatic difference between chaos and periodic behavior. When periodic, the trajectories become eventually stable, so that the point in phase space moves over previous tracks. When chaotic, the space usually becomes hopelessly "cluttered". This cluttering makes it difficult to ascertain much concerning the fractal.

The Poincare section is obtaining by "strobing" the phase space trajectories, so that the dimensionality is reduced by 1. This is usually done once per cycle of the periodic drive. Drive is normally necessary to overcome the loss of energy due to friction. In the book by Baker and Gollub it is stated that 3 coupled equations are necessary for chaos. This statement denies the original form of chaos, studied by the Russians (such as Chirikov), which in Moon's book is referred to as Hamiltonian systems. In quantum mechanics the Hamiltonian never contains a dissipation term; however, in chaos studies it has been common to modify the canonical equations of Hamiltonian by adding a term due to friction. This was done, for example, in simulating the support constrained pendulum.

The Poincare section causes an nth order continuous time system to be replaced by an (n-1)th order discrete time system. Thus a phase space trajectory ellipse (limit cycle) of dimension 1 becomes a point of dimension 0. If there is chaos, it manifests itself by "splattering" of points in the Poincare map. This splattering is not random; rather the points fall on a "strange attractor". Such an attractor is always part of a system that is fractal. The Poincare section has come to be the preferred and perhaps singlemost effective (in terms of cost) indicator of chaos.

It should be noted that the geometry of real (nonlinear) systems is not that with which we are accustomed by training in the past. Man-made geometry with which we're accustomed is Euclidean. It involves circles, triangles, and the like. The geometry of nature, however, is fractal. To better understand complex systems, the base of our math training in physics will have to be revised.

The pendulum has been an excellent pedagogical tool for several reasons, not the least of which is its traditional role in physics since the Copernican revolution. For one thing, it's equations of motion apply directly to some modern systems, such as the Josephson junction. Additionally, it has some similarities (in differential equation form) to the most common of all maps which show chaos–the logistic map (in iterative form). This importance has been recognized by many. For example, all throughout Baker and Gollub's book, the pendulum is used as the "benchmark" to describe various properties of chaos. Obviously, the pendulum is the benchmark also for the present document; however, as has been noted, there are a variety of chaotic pendulum possibilities. In addition to the conventional rigid planar pendulum, some of the others that are treated herein, to varying degrees, are the following: double pendulum, support constrained pendulum, torsion gravity pendulum, and the Kapitza (inverted) pendulum. Additionally, the leaky pendulum, may show chaos at low levels because of the dripping fluid. (Droplets of water from a faucet can demonstrate chaos in terms of the time between drops.) Because of the considerable importance of the pendulum's equations and the logistic map and several other ones, such as the Lorenz map; and because too few people have a working relationship with them, the following information is provided. Attention is given to computer exercises for which a "picture is worth a thousand words".

4.1 Bouncing Bead

One of the simplest chaotic systems to model with the computer is that of a bead which bounces on a horizontal table that executes vertical harmonic motion. The amount of momentum change experienced

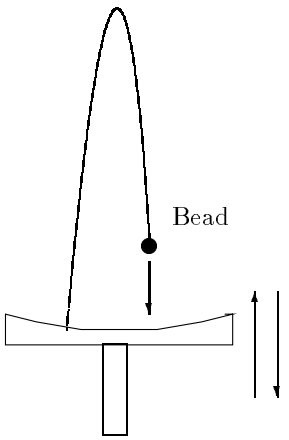

Figure 15: Simple system which can be chaotic—the driven Bouncing Bead.

by the bead is determined by the coefficient of restitution, a . In the present treatment, the motion of the table is considered negligible compared to the average maximum height of the bead's trajectory. Between collisions, the bead is in free fall, influenced only be the fixed acceleration of gravity. The system is illustrated in Fig. 15.

The "strength" of the drive is determined by the table "motion", b . which is a parameter that can be changed in a particularly meaningful way. Using GSM program #2, one may look at the motion (y) vs time, the phase space trajectory (velocity vs y), or the Poincare' section (velocity vs y strobed once per cycle of the drive). For a low drive, typically the bead will settle (after transients have decayed) into a period-1 limit cycle, such as shown in Fig. 16 on the left.

As the drive is increased, a bifurcation occurs; so that the motion becomes period-2 as shown on the right in Fig. 16. Further increase of the drive results in additional bifurcations, as illustrated in Fig. 17.

Notice in the figure that the period-8 case on the right differs from the period-4 on the left in a subtle way. By laying a straightedge across the highest points, it can be seen that the alternate peaks differ in magnitude by a small amount.

Still further increase in the drive results eventually in chaos, as shown in Fig. 18. On the left is a time record of chaotic motion, and on the right is the corresponding Poincare' section. The self-similarity is striking in these cases, and a "full-blown" figure is provided in Fig. 19 to show the details better. This figure was made with a higher resolution graphics than is available in GSM program #2.

It is very educational to look at the modeling in this case. Additionally, if one wants to construct personalized high resolution Poincare' sections, then the following "barebones" code is provided.

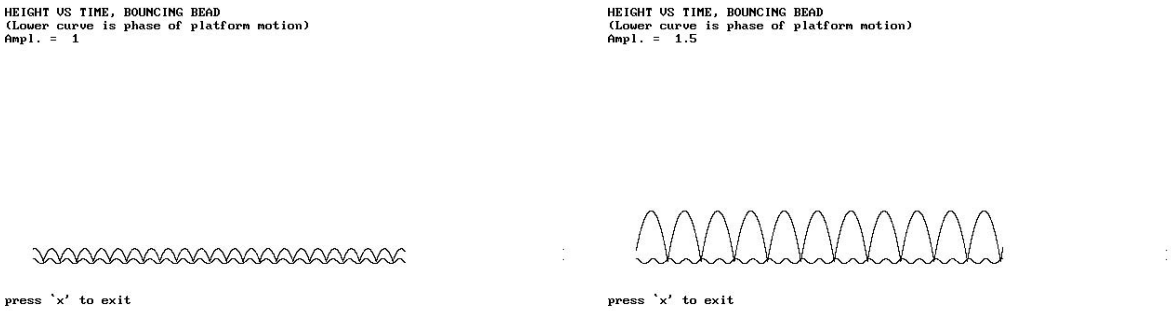

Figure 16: Limit cycles for the driven bouncing bead.

(a). period-1 (b). period-2.

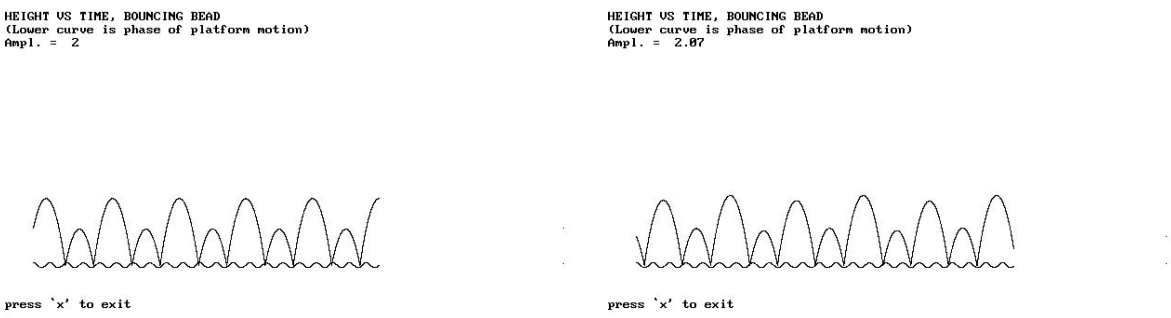

Figure 17: Limit cycles for the driven bouncing bead.

(a). period-4 (b). period-8.

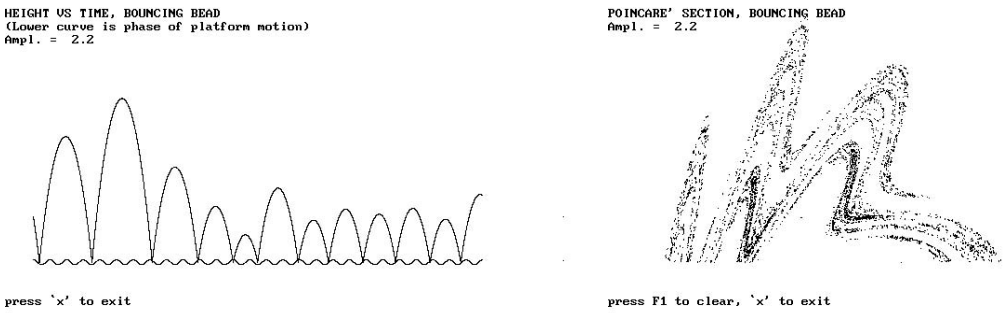

Figure 18: Chaotic bouncing bead.

(a). Motion in time. (b). Poincare' section.

```
SCREEN 12
VIEW (30, 0)-(600, 350): WINDOW (-0!, -0!)-(1, 1)
dt = .01: g = 1
w = 2: a = .7: b = 2
vk = 5
start:
t = t + dt
v = vk - g * (t - tk)
y = vk * (t - tk) - .5 * g * (t - tk) ^ 2
IF y > 0 THEN GOTO 100
tk = t
vk = -a * v + b * (1 + COS(w * tk))
100
dr = COS(w * t)
IF ABS(dr - 1) < .0001 THEN PSET (.065 * v + .25, .015 * y)
GOTO start
END
```

It can be seen from this code that the BASIC language is well suited to modelling of chaos. One should only consider compiled versions, however; because the interpretive basic is far too slow to be useful. The one used in all of this work is QuickBASIC. To execute the program above, one hits 'shift F5'. To exit requires a 'Ctrl break'.

The best way to see the period-doubling route to chaos is by looking at the Poincare' sections ('s' in GSM program #2). The following values of b will show the doubling: 1, 1.5, 2, 2.07, and 2.2. These correspond, respectively to period-1, period-2, period-4, period-8 and chaos. Between 2.07 and 2.2 there is probably a period-16 to be seen (and even higher modes), but it is generally difficult to easily represent the larger modes without a change of scale.

For one who is interested in more details concerning this system, particularly some experiments that have been performed; a good reference is that of N. B. Tufillaro, T. Abbott, and J. Reilly, *An Experimental Approach to Nonlinear Dynamics and Chaos*, Addison Wesley, Redwood City, California (1992).

Figure 19: Fractal Geometry of the Chaotic Bouncing Bead.

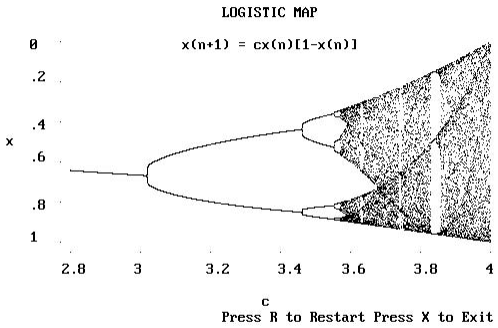

Figure 20: Plot of output from the Logistic equation.

4.2 Logistic Map

A notable characteristic, just demonstrated, was the period doubling route to chaos in the bouncing bead. This is a common route to chaos for a variety of systems which differ considerably in their physical properties. The first occasion to see period doubling was in the logistic (quadratic) map, which is as follows.

$$x(n+1) \;=\; c\; x(n)\; [1 - x(n)] \tag{7}$$

Observe that it is a nonlinear expression because of the quadratic term. The equation is iterative; i.e., the updated value of x (left hand side, LHS) is obtained by working with the present value of x in the indicated operations of the RHS. This seemingly trivial expression possesses a wealth of properties that were not recognized until after the invention of the computer. Feigenbaum even found a fundamental constant associated with the period doubling features of the map. The reason for the name is that population dynamics (such as of insect numbers) can be explained in part with it. When $x(n)$ is small, the $c\,x(n)$ (positive) term is dominant (corresponding to population growth). With continued increase, however, the $-\,c\,x(n)^2$ term will eventually become dominant. The period doubling route to chaos of the logistic map becomes recognizable as one plots $x(n+1)$ as a function of c. Subsequent to a change in c, plotting should be delayed for settling of transients. Fig. 20 shows the usual graph of x vs c. Notice that x values lie in the range 0 to 1.
As c increases above 3, the first period doubling occurs at about 3.02; so that x shows two values for a given c. Iteratively, there is cycling between the two values. Thus the equation repeats every 2nd iterate, which explains the term, period doubling. Later, at about 3.46, each of the branches bifurcates to give 4 values for a given c. The cycling among them repeats every 4th iterate; so the "dynamics" is referred to as a period-4 limit cycle. The period doubling continues on to chaos just below 3.6. Note also the prominent window (period 3) near 3.84, in the middle of the chaotic region. To investigate these features on your own, select and study the Logistic Map (GSM program #16).

A number of physical systems, such as the pendulum, also exhibit period-n limit cycles. These represent subharmonic motions, which are not possible with a linear system. For example, a period-2 limit cycle of the pendulum is one in which the time required for the bob to repeat its motion is twice as long as that of the drive torque. This type of response is easily recognized in the phase space representation. For period-1 the motion is an ellipse at small amplitues, which through Poincare sectioning (strobing) reduces to a point. When the system bifurcates (the term meaning two mathematical solutions) to

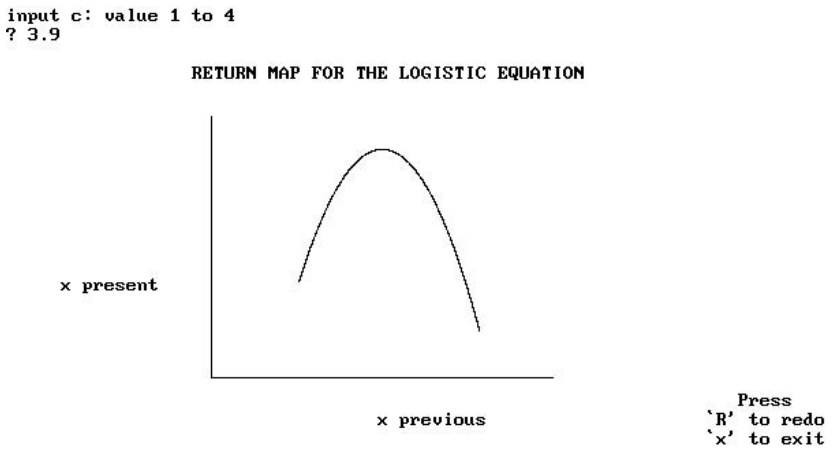

Figure 21: Sample Return map for the Logistic equation.

period-2, then the ellipse becomes a "loop-in-the-loop"; and the single point becomes two points. In the period doubling route to chaos, the Poincare sequence is one of 1-2-4-8-.... unto chaos; in which there is, in effect, an infinity of points but not randomly distributed. Instead, the points on the phase space torus comprise a fractal; i.e., the dimensionality of the space is fractional. The resulting self-similarity means that a view of the space produces essentially the same picture no matter what the magnification. This has been likened unto the view of a very irregular coastline either from a great distance or a near distance, and how essentially the same picture results.

4.3 Return Map

Ed Lorenz (discoverer of chaos with his model of atmospheric convection) was one of the first to use another powerful computational technique for recognizing limit cycles and chaos—the return map. To obtain this map for the logistic equation, one simply plots the previous value of x against its present value. An example is illustrated in Fig. 21 (case shown being chaotic).

(For multi-variable systems the same can be done with one of the variables.) As in other cases, one needs to wait for transients to decay after initializing the algorithm. For the logistic return map the following values of c are noteworthy: 2.9, 3.2, 3.5, 3.56, 3.61, 3.8, 3.84, and 3.9. They give respectively: period-1, period-2, period-4, period-8, chaos (2 segment), chaos, period-3 (window), and chaos. When executing the program (GSM program #27), hitting "r" on the keyboard allows one to quickly run through the period-n and chaotic cases just cited.

4.4 Logistic Map, Graphical Representation

For one who is greatly benefited by visual (graphical) representations, the logistic map can be better understood by means of GSM program #15. This program uses a type of graphical generating function. The inverted parabola is shown in the graph, and the iteration involves straight line segments between the parabola and the 45 degree line, corresponding to $x(n+1) = x(n)$. One can readily see the difference between period-n limit cycles and chaos with this program. For a limit cycle, a stable figure will develop, once transients have settled; if chaotic, this never happens. To see the pattern after transients, hold "c" on the keyboard to clear the screen's previous traces. An example output is shown in Fig. 22.

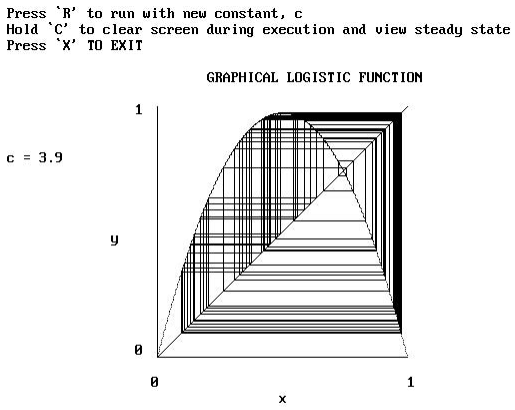

Figure 22: Graphical representation of the Logistic map.

4.5 Entropy of the Logistic Map

One of the most powerful concepts in all of physics is that of entropy, given to us by Boltzmann, and which is the basis for statistical physics. In statistical mechanics, entropy is defined as S = k log W where W is the number of states available to the system, and k is Boltzmann's constant. This quantifier of "disorder" is the basis for obtaining the equation of state of a thermodynamic system using quantum mechanics. In descriptions of chaos, such as the logistic equation; k is typically set to 1 because the number of states is so small. By contrast, in macroscopic physical systems Avogadro's number may be representative. In the logistic equation, when there is only 1 solution, the entropy is 0 since Log 1= 0. After bifurcating (meaning more than one mathematical solution) to 2 solutions, the entropy becomes 0.693 = Log 2. The period doubling route to chaos continues with S = 1.386, 2.079, 2.773, ... , where the upper limit is determined (computationally) by the number of values that one is willing to wait for during accumulation into bins.

In program #9, only 20 values maximum per bin is used. Thus the maximum value of the entropy is 3, during chaos. Especially interesting is the entropy (ordinate labeled S/k in the graph which is generated) corresponding to the window at c = 3.84. As noted before, this window is period-3; therefore the entropy should be 1.099, which is seen in Fig. 23 to be essentially the value as determined by the algorithm.

4.6 Synchronized Logistic Maps

In a study by John Masten and R. Peters (publication in review), two coupled logistic maps were studied from the view of synchronism. Although work has been done on coupled logistic maps in the past, the efforts have centered around the chaotic characteristics of the coupled systems and not on synchronization. The present work considered the following equations:

$$x_{n+1} = c[(1-a)x_n + ay_n][1-((1-a)x_n + ay_n)] \tag{8}$$

$$y_{n+1} = cy_n(1-y_n) \tag{9}$$

A value of zero for "a" decouples the two equations and results in two independent logistic maps, whereas a value of one results in total coupling. The system was studied using bifurcation diagrams, entropy plots, synchronization plots, and Lyapunov exponents. It was found that synchronization was

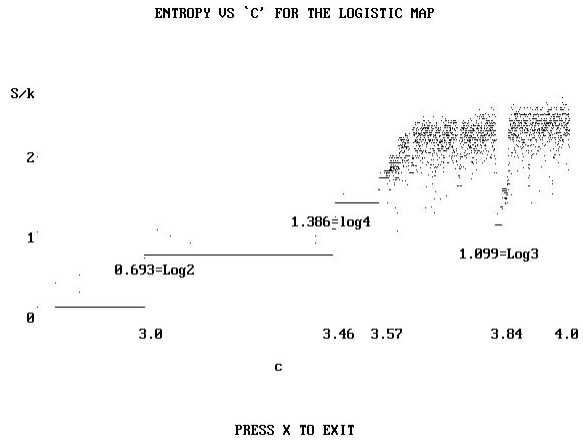

Figure 23: Entropy of the Logistic map.

possible over large regions of operation, even though individual dynamic variables within a region might be chaotic.

4.7 Lyapunov Exponents for the Logistic Map

These exponents are named after the Russian mathematician who lived from 1857 to 1918. We compute them for the Logistic map by considering the generating function, $f = cx(1-x)$. The 2nd iterate can be written as

$$x_{n+2} = f[x_{n+1}] = f_2[x(n)] \tag{10}$$

and this generalizes to

$$f_N[x(n+\epsilon)] - f_N[x(n)] = \epsilon\, e^{\lambda\, n} \tag{11}$$

More commonly the exponent is referenced to base 2 rather than base e (inverse of the natural logarithm). Taking the logarithm of both sides of the equation gives

$$ln([f_N(x_n+\epsilon) - f_N(x_n)]/\epsilon) = \lambda n \tag{12}$$

which is recognized, on the left hand side as $ln\frac{df_N}{dx}$ in the limit as $\epsilon \to 0$. Now consider the derivatives. Letting $u = f[x(0)]$,

$$\frac{df_2 x(0)}{dx} = \frac{du}{dx}\frac{df(u)}{du} = f'(u)f'[x(0)] = f'[x(1)]f'[x(0)] \tag{13}$$

and in general

$$\frac{df_N[x(0)]}{dx} = f'[x(n)]f'[x(n-1]f'[x(n-2)]....f'[x(0)] \tag{14}$$

This result, with the properties of the logarithm, allows us to solve for the Lyapunov exponent

$$\lambda = \lim_{n\to\infty} \frac{1}{n}\sum_{i=0}^{n-1} ln|f'(x_i)| \tag{15}$$

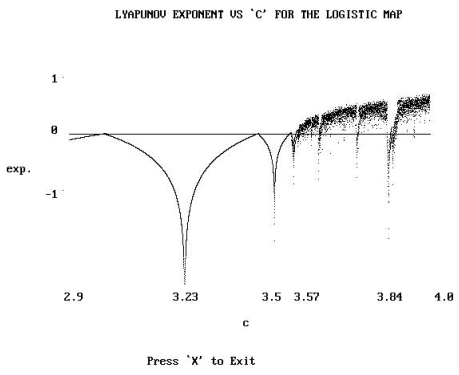

Figure 24: Lyapunov exponent for the Logistic map.

In evaluating the Lyapunov exponents computationally, it is usually sufficient to approximate the infinite sum by 100 terms, which was done in the code of GSM program #22. Fig. 24 was produced with this program.

Note the positive value of lambda above 3.57 corresponding to chaos, except that it drops below 0 at a few places such as c = 3.84 (the period-3 limit cycle). Also the deep negative value at 3.23 is noteworthy. Whereas the condition for chaos is exponential divergence of closely spaced phase trajectories (positive lambda) we see that c = 3.23 is a case of strong convergence.

4.8 Circle Map

The circle map is useful for understanding "winding", Arnold tongues, and the "devil's staircase". Also sometimes called the sine-circle map or the standard map, it has been shown that there are a range of parameters over which it can be correlated with pendulum motion [M. H. Jensen, P. Bak, and T. Bohr, Phys. Rev. A *30*, 1960 (1984)]. Much of the theoretical understanding of this map is due to the Russian mathematician, V. I. Arnold, [c. f. *Geometric Methods in the Theory of Ordinary Differential Equations*, Springer, New York (1983)]. A good, detailed introductory description of the map is that by Robert C. Hilborn, [*Chaos and Nonlinear Dynamics, An Introduction for Scientists and Engineers* p. 263 (1994)]. The circle map can be expressed in terms of angle (mod 2π), but it is usually normalized as follows:

$$\theta_{n+1} \;=\; \theta_n \;+\; \Omega \;-\; \frac{K}{2\pi}\; sin\;(2\pi\theta_n)\;(mod\;1) \tag{16}$$

The parameter, $K > 0$, determines the amount of nonlinearity; and Ω is the frequency-ratio parameter.

To study this map, use TELAWARE'S GSM program #6. Fig. 25 shows an example in which phase locking has occurred.

To better understand phase, or frequency locking, which is the hall-mark of this map with non zero K ; we define the winding number, as

$$w \;=\; \lim_{n\to\infty} \frac{\theta_n \;-\; \theta_0}{n} \text{without taking mod 1} \tag{17}$$

In GSM program #6, only 20 iterations are used in estimating the winding number by this means. If the graph, for a given given input of K and Ω is stationary after pressing F1, then locking has occurred. The printed winding number, w may be used to determine the periodicity of the motion in terms of a ratio of integers p/q as follows. The number of horizontal segments (iteration number) is equal to q . Multiplying q by the printed fraction for the winding number gives the number of

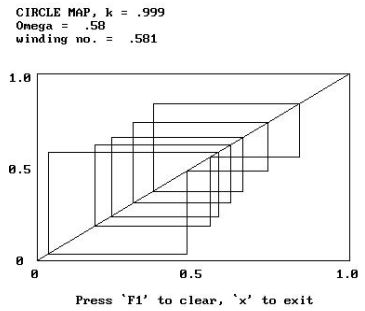

Figure 25: Example of phase locking in the circle map.

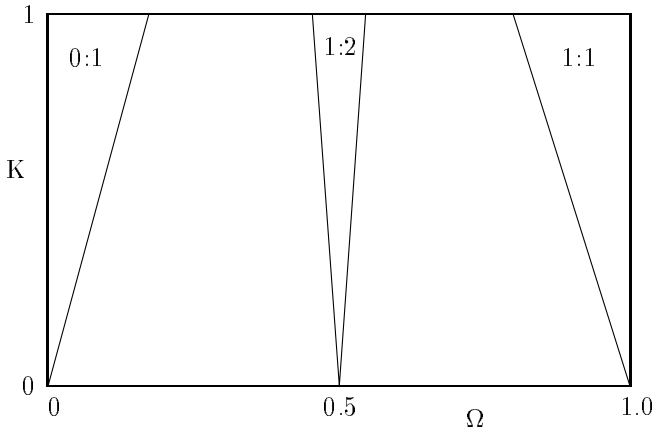

Figure 26: Three Frequency Locked regions known as Arnold Tongues.

rotations, p before θ repeats. Because the calculation of w involves only 20 iterations, the p estimated this way may differ from an integer slightly—thus round it accordingly.

Thus for the example of Fig. 25, there are 12 iterations and $w = 0.583$. Thus the motion is one associated with a $7 / 12$ Arnold tongue.

The value of K at 0.999 has been selected, as in all cases here considered, less than 1. Beyond 1 (a critical value), several different periodic oscillations can occur for given (K, Ω) depending on initial conditions. The map is thus noninvertible, which is a condition that is necessary for chaos.

The regions of locking are especially interesting when one plots K vs Ω as illustrated in Fig. 26. The central region, identified by $\frac{1}{2}$ does not really have straight line borders as shown, but rather they are curved inward slightly. There are a whole lot of tongues other than the ones shown, and they can be identified using GSM program #6. The indicated example of phase locking, for instance, is just one. Some other interesting cases are as follows. Using $K = 0.999$, input the following values of Ω : 0.1, 0.28, 0.35, 0.41, 0.5, 0.59, 0.65, 0.72, *and* 0.9 . In so doing, you will find the following periodicities: 0/1, 1/4, 1/3, 2/5, 1/2, 3/5, 2/3, 3/4, *and* 1/1 respectively. Although the w values printed by the program will be fractions, you can show that they correspond to the indicated ratio of integers, by the method mentioned above.

When $K = 0$, the only way periodicity is possible is for the value of Ω to correspond to a ratio of integers. In the left side of Fig. 27, $\Omega = \frac{7}{12}$ "exactly", and the winding number, as readily

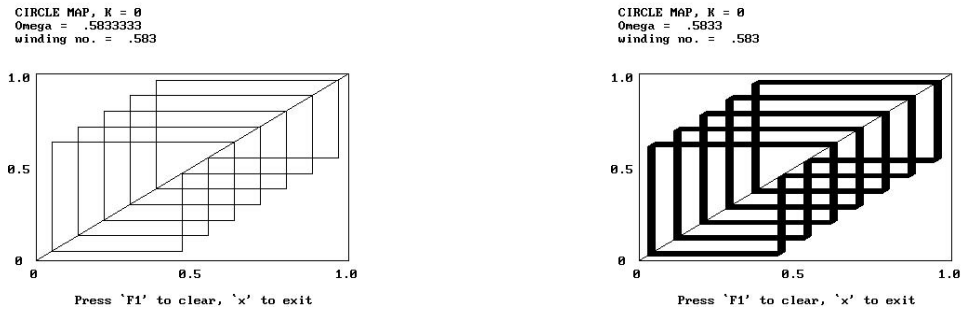

Figure 27: Example results for the linear circle map (K = 0).

(a). With a rational winding number (b). With a slightly irrational one.

demonstrated for the linear case, is just this ratio of integers. If Ω differs only slightly from the ratio, as shown on the right side of Fig. 27, then quasi-periodicmotion results.

If one holds the nonlinearity parameter constant at $K = 1.0$ and lets Ω vary smoothly from 0 to 1; and then plots w vs Ω, then the "devil's staircase" results, as shown in Fig. 28. This graph was generated with GSM program #29. (For these calculations, 200 iterations were used per evaluation of w.)

4.8.1 Mode Locking in Lasers

Undoubtedly the circle map is similar to some physical systems, when it comes to frequency locking. One of the best known examples is with certain lasers. The following comments are taken from A. Yariv, *Optical Electronics, 3rd ed.*, Holt, Rhinehart and Winston, New York (1985). "Mode locking occurs spontaneously in some lasers if the optical path contains a saturable absorber (an absorber whose opacity decreases with increasing optical intensity). This method is used to induce mode locking in the high-power pulsed solid state lasers, and in continuous dye lasers. This is due to the fact that such a dye will absorb less power from a mode locked train of pulses than from a random phase oscillation of many modes; since the first form of oscillation leads to the highest possible peak intensities, for a given average power from the laser, and is consequently attenuated less severely." Expressed more simply, "... the presence of a saturable absorber in the laser cavity will 'force' the laser, by a 'survival of the fittest' mechanism, to lock its modes' phases."

4.9 Peters Map and Chirikov Map

The Peters Map was discovered following studies, both theoretical and experimental, of the torsion-gravity pendulum. Modification of the differential equations was accomplished by comparing with the Chirikov map. The Chirikov map is related to the conventional pendulum, which can be seen by starting with the equations of motion in Hamilton's form, as follows

$$\frac{\partial H}{\partial p} = \dot{q} \quad , \frac{\partial\ H}{\partial q} = -\dot{p} \tag{18}$$

$$\frac{p}{I} = \dot{q}\ ,\ mgL\ sin\ q = -\dot{p} \tag{19}$$

If one sets the time differential, dt, to 1 after putting the equations in dimensionless form; then the equations which generate the Chirikov map results.

$$p \leftarrow p - c\ sin\ q\ ,\ q \leftarrow q + p \tag{20}$$

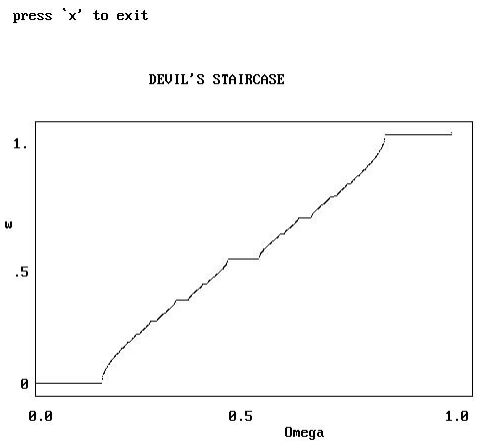

Figure 28: The Devil's Staircase.

In like manner, the equations of motion for the torsion-gravity pendulum are given by

$$\frac{\partial H}{\partial p} \; = \; p/I \; = \; \dot{\theta} \; , \frac{\partial H}{\partial \theta} \; = \; k\theta \; - \; mgL \; sin\theta \; = \; -\dot{p} \tag{21}$$

Setting dt = 1 after normalizing gives the equations which generate the Peters map. $p \; \leftarrow \; p \; - \; q \; + \; c \; sin \; q \quad , \quad q \; \leftarrow \; q \; + \; p$. These expressions are similar to the Chirikov map except for the addition of $-q$ and the change of algebraic sign on the sine term. There is considerable versatility in this set of equations. When c is small, they reduce to the simple harmonic oscillator. When c is in the neighborhood of and less than 1.5 they give the Duffing system. When c is large they correspond to the pendulum. Using the software program #24, one can readily study the cases for c small up to about 5. When $c = 1.6$ and larger the map shows fractal features with inversion symmetry, as illustrated in Fig. 29 (left side). Observe that periodic boundary conditions are used, so that both q and p are mapped into $\pm \, \pi$. The Chirikov map is quite sensitive to the initial (starting) values of q and p , which in the software program #5 increase monotonically in a loop. Each looping operation plots 1000 (q, p) points between re-initializations.

4.10 Henon Map

The map given to us by French astronomer Henon is the following:

$$x(n+1) \; = \; 1 \; - \; a \; x(n)^2 \; + \; y(n) \quad , \quad y(n+1) \; = \; b \; x(n) \tag{22}$$

The famous set of points shown in Fig. 30 is not obtained by the usual process of simply initializing x and y and then iterating to produce the fractal. Rather, GSM program #11 first fills an array of x,y points using the random number generator of QBasic. Only after the array has been filled is the fractal generated using the array values in the above pair of equations.

4.11 Henon-Heile Problem

Not only was Henon responsible for the discrete map of eqns. 22, he also worked on a problem with Heile which has applications in cosmology (galaxy dynamics). The following set of equations is considered in Koonin's book on computational physics.

$$\frac{d \; P_x}{dt} \; = \; - \; x \; - \; 2 \; x \; y \quad , \quad \frac{dx}{dt} \; = \; P_x \tag{23}$$

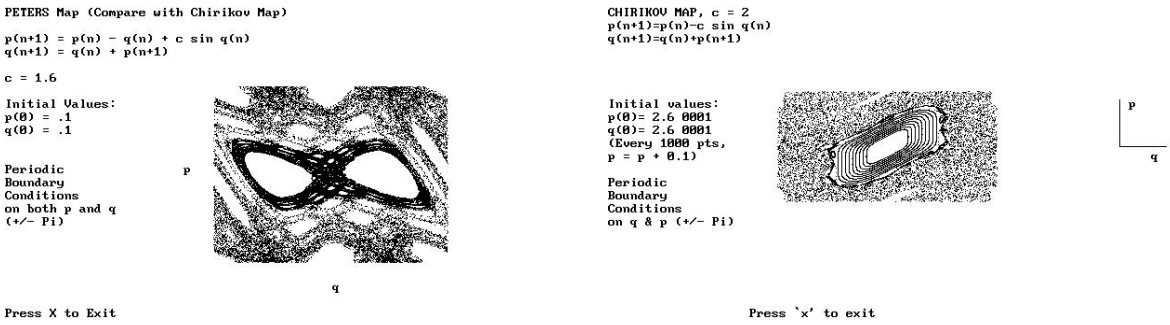

Figure 29: Example cases of Peters map (left) and Chirikov map (right).

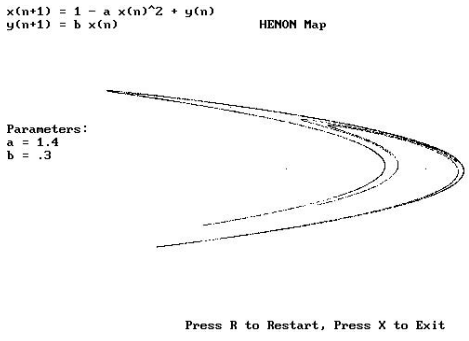

Figure 30: Henon map.

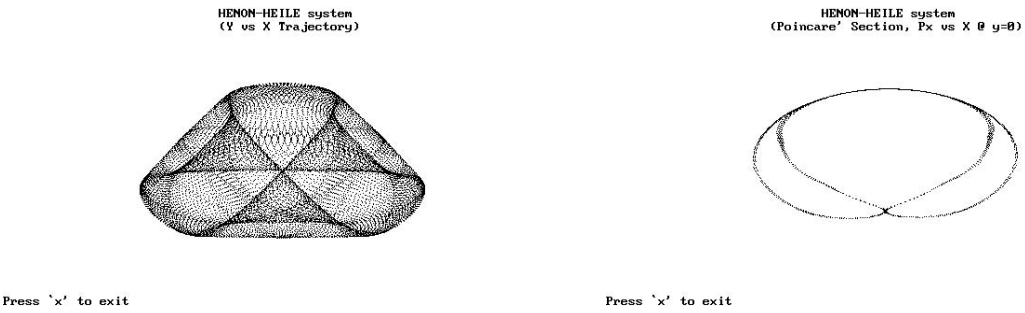

Figure 31: Output from Henon-Heile: on the left is a phase plot, on the right a Poincare' section.

$$\frac{d\,P_y}{dt} \;=\; -\,y \;-\; x^2 \;+\; y^2 \quad , \quad \frac{dy}{dt} \;=\; P_y \tag{24}$$

There are 4 first order differential equations, and the coupling is strictly in the momentum terms. The nonlinearity is from the quadratic terms in x and y and also the product, xy in the P_x derivative. Koonin integrates the equations, first the $d\,P_x/dt$ and $d\,P_y/dt$ pair, followed by the dx/dt and dy/dt pair, using Runge Kutta. In the present program, Henon-Heile, the integration is done using the Cromer-Euler algorithm, as in all other cases involving integration in the routines that are part of this monograph. The trajectory generated with the program has a 3-fold rotational symmetry as shown in Fig. 31 (left). This is a consequence of the Henon-Heile potential (an equilateral triangle in the limit). The program produces a graph that is either a phase space trajectory or a Poincare' section. Unlike the pendulum Poincare section, which is produced by strobing at the frequency of the drive, this Hamiltonian system does not have a drive; since there is no friction. Thus to provide the section, one plots Px vs x as y passes through 0. This technique was used in generating Poincare sections for the support constrained pendulum, which is chaotic in the limit of zero damping (drive removed). A Poincare' section generated by GSM program #10 is shown in Fig. 31 on the right.

4.12 Solar System related

It was mentioned that the Henon-Heile problem came about from the study of cosmology. There are other examples of chaos from astronomy, not only in galactic systems, but also in our own solar system. One of the best known cases, discovered by Voyager 2, is the chaotic rotation of Hyperion. One of the satellites of Saturn, Hyperion is a biscuit-shaped chunk roughly 350 km across and 200 km thick [W. K. Hartmann, *Astronomy: The Cosmic Journey*, Wadsworth, Belmont, CA, p. 259 (1991)]. Due to complex forces acting on its irregular shape, its rotation is chaotic.

4.12.1 Poincare's astronomy

Not only does astronomy continue to influence the world of chaos, but the science actually had its beginning with the three-body gravitational problem. It was Poincare' who realized that the 3-body case could not be solved analytically. In fact, the only reason we can solve the 2-body problem is because we convert it to an equivalent 1-body case. This is, in fact, the basis for the concept of the "reduced mass". Poincare' realized that nonlinearity is the paradigm for most of nature's behavior. He couldn't do much to advance the cause of chaos, however, because he didn't have a computer. More particularly, he didn't have computer graphics to generate the pictures that have become so important to its study.

Because of its historical importance, a gravitational program is included in the Telaware package. As treated, the three body problem (program #37, is extremely artificial. First of all, two of the three objects are fixed, which is clearly impossible in nature. Second, there is a modification to the force between these two objects and the moving third one when it gets very close. The inverse square law of

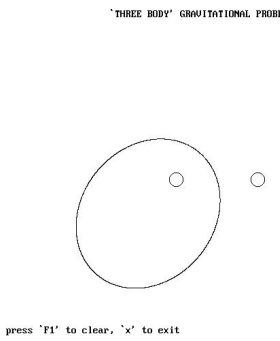

Figure 32: Example of 2-body motion—a Keplerian elliptical orbit.

the gravitational attraction becomes unmanageable when the distance, r, gets very small. To compensate for "blow-up" in the code, the following is done. When $r < r_c$, the momentum of the moving object is maintained fixed at the value it had just before penetrating the critical area (tantamount to turning off the force). In constructing the code, r_c was adjusted by trial and error until "reasonable" performance was realized.

4.12.2 Kepler problem

For a better appreciation of the 3-body problem, it is recommended that one first look at the 2-body case. This can be done by setting the mass of either of the fixed bodies at 0. What results is an ellipse, the orientation of which can be varied somewhat according to the input value of transverse velocity of the moving object, as illustrated in Fig. 32.

The following code illustrates how the 2-body problem would be treated in a stand-alone program.

```
x = -2: vy = .85: v20 = vx ^ 2 + vy ^ 2: y = 0
PRINT "input t = 0 value of transverse velocity to"
PRINT "change orientation of ellipse (-.2 to .2)"
INPUT vx: dt = .01: x0 = 3: y0 = 0
SCREEN 12: CIRCLE (250, 250), 5
start: t = t + dt: r2 = x ^ 2 + y ^ 2: r = SQR(r2): f = 1 / r ^ 2!
fx = -f * x / r: fy = -f * y / r
vx = vx + fx * dt: vy = vy + fy * dt
v2 = vx ^ 2 + vy ^ 2: x = x + vx * dt: y = y + vy * dt
PSET (20 * x + 250, 20 * y + 250): GOTO start
END
```

One of the reasons for showing this is to permit an interesting additional study. If one changes the 2 in f=1/r^ 2 to something different, then precession of the ellipse occurs. Slightly less than 2 yields oppositely directed precession as compared to slightly greater than 2. This illustrates nicely the fact that the square law of gravity is exactly that—to within our abilities to distinguish such a precession from perturbations of other objects within the solar system. *A word of caution is in order. One of the artifacts of the integration technique is that highly elliptical orbits precess at a small rate even when the exponent is exactly 2.*

The 3-body case, because of its artificiality, yields eventually absurd results; i.e., the moving object either escapes or is trapped by one of the two fixed objects. Until this happens, one still can appreciate the sensitive dependence on initial conditions of this system. Once it gets useless, simply press 'x' and rerun. Typically, many cycles are visible before that happens, as illustrated in Fig. 33.

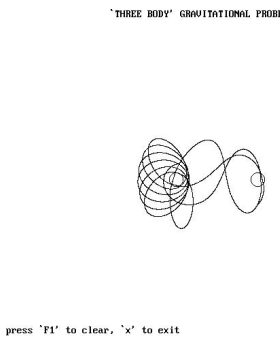

Figure 33: Three body gravitational problem (highly artificial).

4.13 Zany root finder

This program involves a strange attractor in a root finding algorithm. My first occasion to encounter strange attractors was while working at LTV on the U. S. antisatellite program. The algorithm which produced them was a modified Newton-Raphson root finding scheme, applied to Kepler's equation.

4.13.1 Newton's method

Most physics students are familiar with the basic Newton method; i.e., look for a root, x_r , of the transcendental function, $f(x)$, using

$$x_{n+1} \;=\; x_n \;-\; f(x_n)/f'(x_n) \tag{25}$$

where f' is the derivative of f with respect to x . If the function is well behaved, x_r will be the limiting x_n as $n \to \infty$. Depending on how well behaved the function is, and the accuracy required; one may approach acceptably close to x_r after only half a dozen or so iterations. Sometimes, though, convergence is much slower; so an "improved" procedure may be sought.

4.13.2 "Improved" Newton method

The improved Newton method is one that is usually called Chebychev's formula [?].

$$x_{n+1} \;=\; x_n \;-\; \frac{f}{f'}[\,1 \;+\; \frac{1}{2}(\frac{f}{f'})(\frac{f''}{f'})] \tag{26}$$

which results from a second-order Taylor series expansion. Whereas the standard Newton method has quadratic convergence, the improved method has cubic convergence (if it indeed converges).

As compared to the standard Newton method, greater care in initialization is required when using the Chebychev formula. This can be easily illustrated with Kepler's equation, which must be solved to find the position of a planet relative to the sun at a given time.

4.13.3 Kepler's equation

Kepler's equation is

$$f(E) \;=\; E \;-\; e\;sin\;E \;-\; M \;=\; 0 \tag{27}$$

where M is the mean anomaly, e is the eccentricity of the orbit, and E is the eccentric anomaly. The givens are M and e , and E is to be determined. (The steps for determining the position of a planet are as follows: (i) Determine M , which increases at a constant rate (simply related to mean

solar time, in the case of the earth), (ii) determine E by solving Kepler's equation, and (iii) compute the true anomaly from E ; which with the distance from the sun, determines the position.)

There is no closed form solution to Kepler's equation; however, for small orbital eccentricities, many approximation methods have been published, including one of my own [?].

When the Chebychev method is used with Kepler's equation, one must be extremely cautious in initialization, when e is large. It is possible to get into iterative loops that never converge to a solution of Kepler's equation, as was discovered by Broucke [?]. He noted some cases which were, in effect, a period-2 limit cycle, and others that were chaotic. The chaotic cases are ones which he referred to as strange attractors, following the work of Henon [?].

The following code has been used to show that chaos can occur when the Chebychev algorithm is applied to Kepler's equation. Moreover, it has been used to demonstrate the best known route to chaos as a parameter is changed—the period doubling one.

```
CLS
KEY 15, CHR$(0) + CHR$(&H2D)
ON KEY(15) GOSUB terminate
KEY(15) ON
COLOR 7, 1
SCREEN 9
COLOR 15, 4
restart: CLS
PRINT "Input mean anomaly (2.30 to 2.36) (‘r’ to redo, ‘x’ to exit)"
INPUT m
eps = .5436
e = .595
i = 0
start:
i = i + 1
f = e - m - eps * SIN(e)
fp = 1 - eps * COS(e)
fpp = eps * SIN(e)
e = e - (f / fp) * (1 + .5 * (f / fp) * (fpp / fp))
IF i > 100 THEN PSET (1000 * (ep - .35), 1000 * (e - .35))
ep = e
IF INKEY$ = "r" THEN GOTO restart
GOTO start
terminate:
END
```

Observe that plotting is delayed by 100 iterations, so that transients can settle.

This program has been included in the General simulations menu (#42). To exhibit the period doubling route to chaos, input sequentially the following values of mean anomaly: $M = 2.30$, 2.33, 2.345, 2.349, 2.34975, 2.35, *and* 2.36 . (In GSM #42, the eccentric anomaly starting value and eccentricity are fixed at E = 0.595 and e =0.5436 repectively.) What is being plotted (a return map, after transients have settled) is $E_{previous}$ vs $E_{present}$. The seven values of M give, respectively, period-1, period-2, period-4, period-8, period-16, segmented chaos, and full chaos. The full chaos case, using $M = 2.36$ is shown in Fig. 34.

What this illustrates is the following. Imagine one were looking for solutions to Kepler's equation for a limited orbital region of an object (maybe a comet) with eccentricity $e = 0.5436$. The mean anomaly is smoothly varying during this time, through the values indicated above (not a big range). If the Chebychev algorithm were used to try and determine E , and the same starting value ($E_{guess} = 0.595$) were used everytime to initialize the algorithm, then 6 out of 7 of the attempts at a meaningful solution would fail.

What this should point out to students is: BEWARE, when working with numerical algorithms. Powerful techniqes can sometimes be afflicted with absurd results, if limitations are not understood. It's

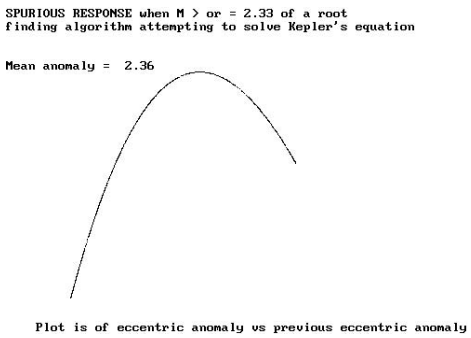

Figure 34: Chaotic spurious solution to Kepler's equation.

always good to check for self-consistency, rather than blindly believing output.

References

[1] F. B. Hildebrand, *Introduction to Numerical Analysis*, McGraw-Hill, New York (1956).

[2] R. Peters, "Rapidly converging series approximation to Kepler's Equation", AAS/AIAA Specialty conference, paper AAS 83-396, Lake Placid, New York (1983). It's also possible to avoid Kepler's equation altogether; c.f., R. Peters, "True anomaly approximation for elliptical orbits", J. Guid. Control and Dynamics *14*, no. 5, 1069 (1991).

[3] R. Broucke, "On Kepler's Equation and Strange Attractors", J. Astr. Sci. XXVIII (3), 255-265 (1980).

[4] M. Henon and Y. Pomeau, "Two Strange Attractors with a strange structure", in "Lecture Notes in Math.", No. 565, Springer Verlag, 29-68 (1976).

4.14 Kapitza Pendulum

In the United States we typically refer to this pendulum as the inverted pendulum. Its stability derives from the rapid oscillation of the support. GSM PROGRAM #12 was used to generate the plots of Fig. 35.

4.14.1 Some Kapitza history

There's an interesting story behind the Kapitza pendulum, heard during a visit to Novosobirsk State University in 1993. High energy theorist, Valery Serbo (who supplied the adjective, "crucial" for one version of SDC sensors), is the one who told the story. Because Kapitza was a dissident during the Stalinist regime, he was "sentenced" to his dacha. (None of the politicians was willing to contemplate imprisonment of this man—he won the Nobel Prize in 1978 for his studies of liquid helium.) This did not stop Kapitza from doing physics, as shown by the statements from his article, "Dynamical stability of a pendulum when its point of suspension vibrates" [P. L. Kapitza, Zhur. Eksp. i Teoret. Fiz., *21*, 588 (1951)]; Collected Papers, ch. 45, p. 714]:

"It is well known that for a body at rest the most stable state is the one in which the centre of gravity of the body is in the lowest position (corresponding to the minimum potential energy), whereas in a dynamical equilibrium the most stable is a state in which the centre of gravity is in the highest position (corresponding to the maximum potential energy)."

"An ordinary top is the most striking example of this principle. As is known, the force caused by the friction of the top's foot against a surface makes the top axis rise and assume the most vertical position, the precession is damped and the top is as if being led to a standstill. But besides classical cases of dynamical stability arising from gyroscopic forces a number of other cases are analysed in the literature. For instance, it has been pointed out that in a rapid motion of a man on stilts, on a bicycle, in a bus, train and so on, the most stable state is reached when the centre of gravity assumes as high as possible a position."

"One of the best examples of dynamical stability is the pendulum with the oscillating suspension point. In a demonstration, this phenomenon is not less striking than the top, and a study of it is as instructive as that of the top. Nevertheless, this case is not only little investigated but usually it is mentioned neither in text-books nor in treatises on mechanics. In the present work we shall give a simple obvious method of analysing this phenomenon, and describe a device for demonstrating it."

I've observed a remarkable instrument built according to Kapitza's specifications, and also been privileged to meet one who is a beautiful example of generational continuity. A visit to Los Alamos National Laboratory in August 1993 was the occasion of the 50th anniversary of the J. Robert Oppenheimer Memorial Lectures. The speaker was Pyotr Kapitza's son—distinguished Russian physicist, Serguei P. Kapitza. His lecture topic: *"Our Nonlinear World"*. Since 1953, he has been (i) senior scientist and head of the Physics Laboratory of the Institute for Physical Problems of the Russian Academy of Sciences; (ii) since 1965, he has held the chair of physics at the Moscow Institute for Physics and Technology; (iii) since 1973, he has been a moderator for the major Russian television program on science and society; (iv) he has been president of the Physical Society of the USSR; and (v) in 1980, he was awarded the Soviet Union's State Prize. Internationally, he is on the editorial board of *Nature*. His lecture dealt with chaos, concentrating on the topic of population numbers throughout the history of mankind (compare with the logistic equation and other concepts presented in this monograph). Truly, this is an expression of Philip Anderson's statement (in part I, Introduction, of this monograph): "Almost without exception, the more eminent, the more deeply committed, the more successful within a given field a scientist is, the more eager that scientist is to relate to scholars outside his or her field."

The studies by P. L. Kapitza of the inverted pendulum are an interesting example of how theory and experiment might better work together. One can use GSM program #12 to illustrate a number of features of the system. To truly understand the physics requires more than trial and error executions of the software. Rarely, for example, would one find out the following properties, discovered by Kapitza in his theoretical treatment.

Kapitza used the following assumptions: (i) the amplitude of the oscillations of the suspension point is small in comparison with the length of the pendulum, and (ii) the angular frequency of the oscillations of the suspension point is large in comparison with the angular velocity of the oscillations of the pendulum. (These are also reasonably valid in the present software.) From these came the following conclusions: The suspension-point oscillations give rise to a torque whose magnitude does not depend explicitly on the time and pendulum length and is determined by the pendulum mass and the square of the velocity of the suspension-point oscillations. The torque tends to set the rod of the pendulum in the direction of the axis of the suspension point oscillations.

He even went on to speculate, as the results of these studies, on the "possibility for observing the aligning effect of the vibrational moment on colloidal particles and molecules."

4.15 Conventional Pendulum

Software dealing with the conventional pendulum has been treated at length in part I of this monograph, with the exception of the pendulum emulator, GSM program #23. Shown in Fig. 36 is an output of this program, the "heart" of which was written by David Mehrl of the Electrical Engineering Department at Texas Tech University.

4.16 Lorenz Model of Convection

Ed Lorenz started all this business by noting the "butterfly effect" in the equations he was using to model atmospheric convection. Based on the Navier-Stokes equations of fluid dynamics, his equations

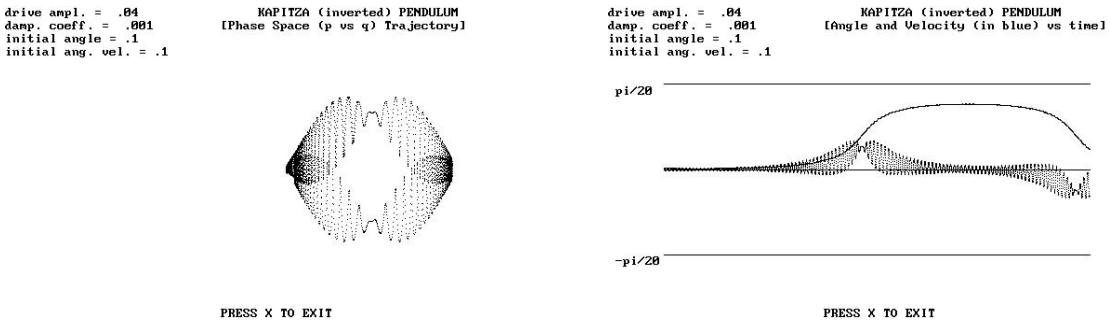

Figure 35: Kapitza pendulum simulation results: left is phase space, right is time plot.

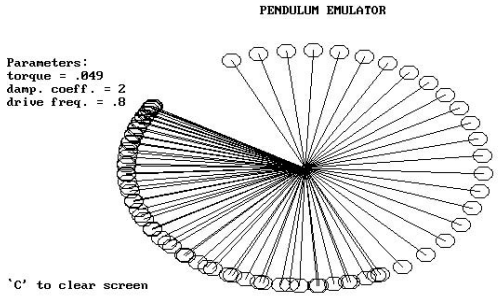

Figure 36: Example output from the pendulum emulator.

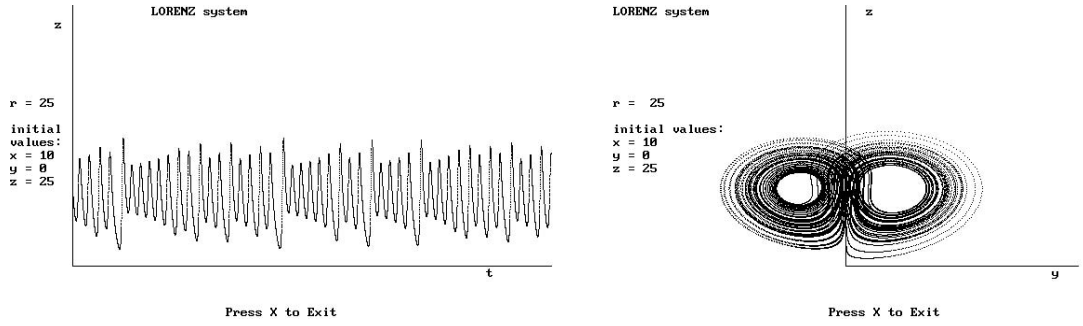

Figure 37: The Lorenz model of convection.

(a). Time dependence of z. (b). phase trajectory, z vs y.

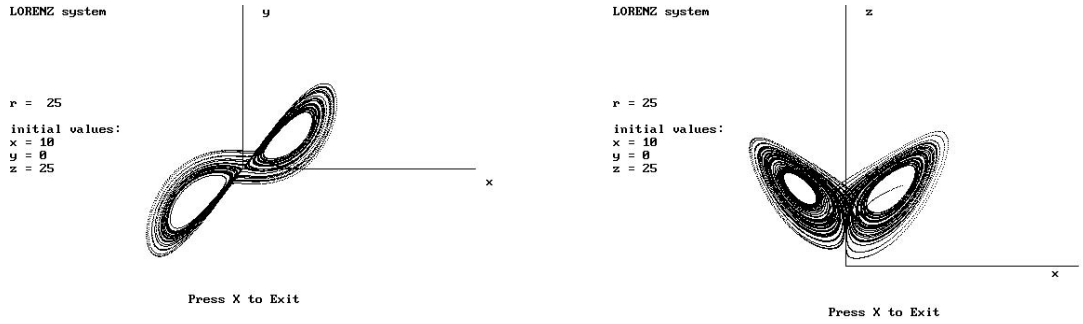

Figure 38: Phase space trajectories, the Lorenz model of convection.

(a). y vs x. (b). z vs x.

are highly nonlinear. Before looking at the math specifically, let's note the famous trajectories shown in Figures 37 and 38. These were generated with GSM programs #18 through 21,
using the Cromer-Euler algorithm on the following equations:

$$\dot{x} \;=\; 10\,y \;-\; 10\,x \tag{28}$$

$$\dot{y} \;=\; -x\,z \;-\; y \;+\; 24\,x \tag{29}$$

$$\dot{z} \;=\; x\,y \;-\; \frac{8}{3}\,z \tag{30}$$

4.16.1 Thermal Soaring in Gliders

It is worthwhile considering a little of the physics involved in the Lorenz equations, from the perspective of a glider pilot. When the earth is heated, beginning in the morning, the atmosphere does not absorb much solar radiation. It is warmed primarily by contact with the earth's surface. Having lower density, the warmed air rises; as every good physics student understands by Archimedes principle. However, we

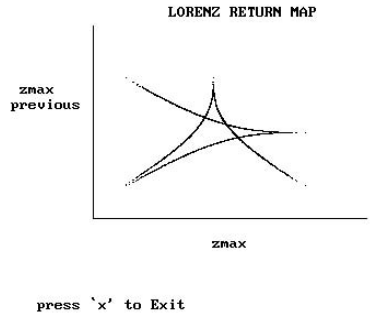

Figure 39: Return Map for the z-variable of the Lorenz equations.

also recognize a conservation feature, embodied within the continuity equation. Specifically, if there is rising air in some regions, then there must also be falling air in other regions. Sailplane pilots try to avoid the latter, because they don't like to walk. As one who has occasionally ventured across sandy soils between Lubbock and Amarillo, Texas; I can attest to the fact that there can be strong sink (hundreds of feet per minute).

Sailplane pilots are also quite familiar with the chaotic features of circulation involving thermal, as opposed to ridge, lift. It's a good thing, because there are no ridges here. When Coronado visited in the 1600's he noted that the terrain was as "flat as the ocean–and occupied by 'cows'[bison], which were, in turn, followed by the 'natives' [Comanches].

The southern high plains, where Lubbock is located, is ideal for thermal soaring; and no two flights are ever quite the same. This is clearly the result of sensitive dependence on initial conditions in the Lorenz equations, and they can be even more nonlinear than usual during spring of each year. I personally discovered that fact several years ago when caught in a system that would have come close to maintaining a Steinway grand aloft. (Although good for soaring, Lubbock can quickly produce strong turbulence, sometimes in the form of tornados.)

Those who are members of the Caprock Soaring Club have two trusty cues, which they rely on heavily when searching for thermals. One is dust devils, which always signify the presence of thermals—they've been known to take the roof off of barns (we usually avoid the ones that big). The other cue is the quintessential soarer—birds of prey like the hawks in this area (preyees, such as sand hill crane, also sometimes soar; they will not let you join them.) You must obey the rules of etiquette, such as establishing the same direction of rotation in the thermal. (I once had a hawk nearly come through the canopy after me for violating this rule. It wasn't malicious—I just didn't see him until accosted.)

I once naively asked a pilot from Reese Air Force base, who was a member of our club, the following question: Do you suppose hawks have something like our variometer, to tell them when they're in lift? I will never forget his answer: Can you tell the difference, when barefoot, whether you're walking on concrete or sand?

4.16.2 Lorenz Return Map

In the discussion of the logistic equation (return map section), it was noted that multi-variable systems can also be treated by this means. The best known case is the return map treated by Lorenz himself. In Fig. 39 is the map in terms of z . Unlike the simplicity of the logistic return map ($x_{previous}$ *vs* x), this map requires that the adjacent maximum values of the variable be plotted one against the other. For one who would like to experiment with possibilities beyond the limits of GSM Program #17, the following "barebones" code is provided.

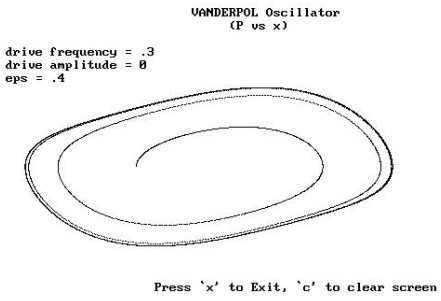

Figure 40: A near linear limit cycle of the van der Pol oscillator (no drive)

```
CLS : r = 24: x = 10: y = 0: z = 25
SCREEN 12: VIEW (0, 0)-(500, 300): WINDOW (-.2, -.3)-(1, 1)
dt = .005: i = 1
start:
t = t + dt: dxdt = 10 * y - 10 * x
x = x + dxdt * dt: dydt = -x * z + r * x - y
y = y + dydt * dt: dzdtp = dzdt: dzdt = x * y - 8 * z / 3
ip = i: IF dzdt < 0 AND dzdtp > 0 THEN i = -i
z = z + dzdt * dt
IF i = 1 AND ip = -1 THEN zmx1 = z
IF i = -1 AND ip = 1 THEN zmx2 = z
PSET (.05 * zmx2 - 1.4, .05 * zmx1 - 1.7)
GOTO start
terminate:
END
```

4.17 van der Pol Oscillator

In Figures 40 and 41 are three phase space trajectories, the first a case not too far from a linear limit, the second a highly nonlinear limit cycle, and the last a chaotic case –all for the van der Pol oscillator. Physically, his oscillator was an electrical circuit (involving adjustable positive feedback). The equation of motion is as follows, where it can be seen that the damping (term multiplying p) can be positive or negative depending on the magnitude of x relative to the parameter ϵ .

$$\dot{p} \;=\; -\,x \;+\; (\epsilon \;-x^2)\; p \;+\; A\; cos\; \omega t \quad , \dot{x} \;=\; p \tag{31}$$

In Fig. 40, the parameter ϵ was set at 0.4, small enough for the phase space trajectory to be a distorted ellipse. Even though the drive is zero, the curve "expands" to steady state from the initial values. In Fig. 41a, the extreme nonlinearity results from the large value of $\epsilon \;=\; 3$. Still the drive is at 0, so the final motion is a limit cycle. In Fig. 41b, a drive($A = 2$) has been added, so that the motion becomes chaotic.

4.18 Duffing Oscillator

The Duffing oscillator (one form) is the classic two well potential. It's Poincare' section, shown in Fig. 42 is well known.

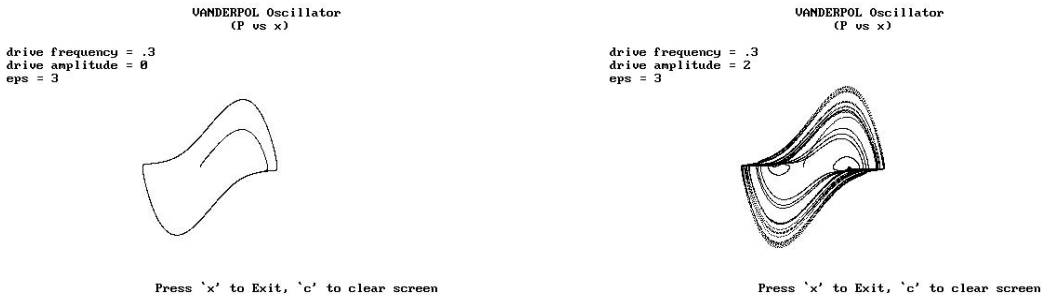

Figure 41: Phase space trajectories of the van der Pol oscillator.

(a). Highly nonlinear, non-chaotic. (b). Chaotic.

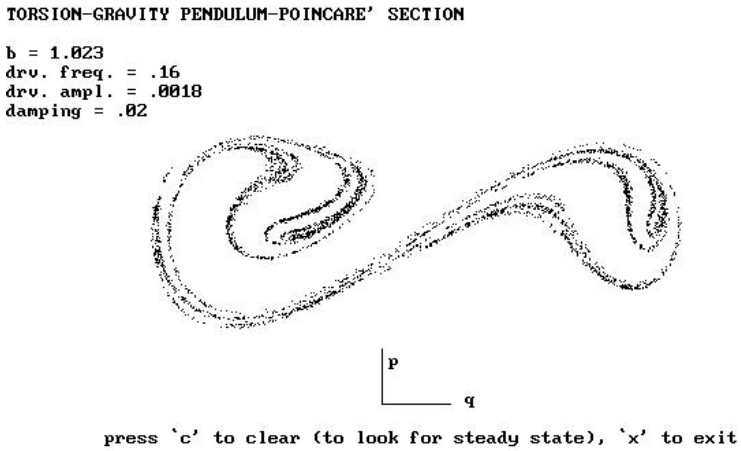

Figure 42: Poincare' section for the Duffing oscillator.

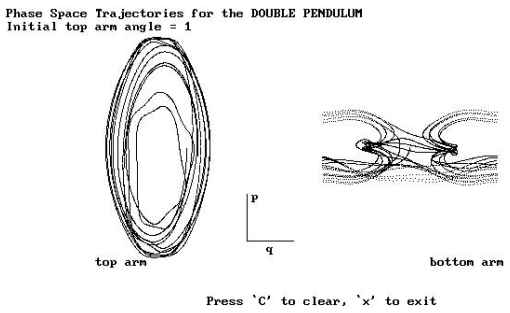

Figure 43: Phase space trajectories for the Double Pendulum.

(a). Top arm motion. (b). Bottom arm motion.

This graph was generated with the simulation for the torsion-gravity pendulum (GSM program #32), which reduces to the Duffing case when the parameter, b, is small (here b = 1.023). In the small b limit, the oscillator presently used is described by the following equation

$$\dot{p} \;=\; a(\theta \;-\; \frac{b}{6a}\,\theta^3) \;-\; c\;p \;+\; A\;cos\;\omega t \quad , \quad a \;=\; b \;-\; 1 \tag{32}$$

$$\dot{\theta} \;=\; p \tag{33}$$

4.19 Double Pendulum

If one takes two physical pendula (solid rods), the top of one connected at a hinge to the bottom of the other, then the system can be chaotic in the limit of zero dissipation. The software that was used to produce Fig. 43 (GSM program #7) was mainly written by Douglass Stevens, using the Cromer-Euler algorithm.

4.20 Classical Harmonic Wave

Before considering any nonlinear wave equations, it's important that the classical case be understood. A lot of students don't appreciate the fact that a classical wave is periodic in both space and time. A hardware demonstration of this dual periodicity is described in the paper by Peters, "Traveling wave pedagogy using an oscilloscope". In lieu of the hardware setup, one may do essentially the same exercises with GSM program #40, whose output is illustrated in Fig. 44.

During execution, observe the simple harmonic motion (y motion in time) of the asterisk, * , which is fixed in the x position. This is like a cork on water, as a wave passes. To understand the kinematic relationship between phase velocity, frequency, and wavelength; one may use a stopwatch with the program. For example, with a 486 Intel (33 MHz), the "velocity" was measured at 1.2 cm/s. The "period" of SHO of * was measured with the stopwatch to be 1.7 s. The "wavelength" was measured (by hitting "pause" on the keyboard) to be 2.1 cm. From these numbers it can be seen that the velocity is the product of frequency (reciprocal period) and wavelength.

The classical wave equation is a linear, 2nd order, partial differential equation (refer to almost any physics textbook). As such, one can construct solutions by using superposition. Finite amplitude waves in real systems are governed, however, by nonlinear partial differential equations. It has been noted that the dislocation kink in a crystal lattice obeys the sine-Gordon equation. This means that the propagation of a pulse-like disturbance from one side, through and to the other side of a crystal (by

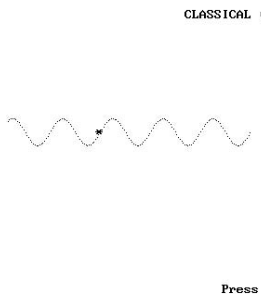

Figure 44: Snapshot of a classical (linear) wave.

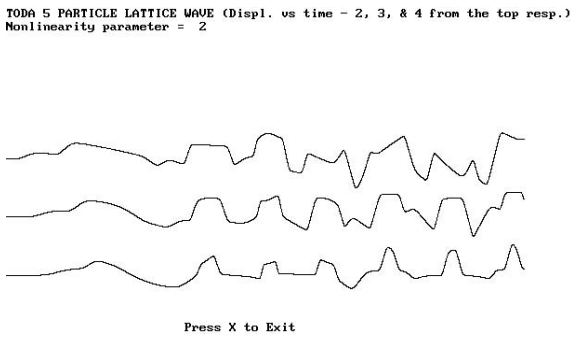

Figure 45: Motion vs time for 3 of the 5 particles of a Toda lattice.

means of the dislocation defects) is an example of a soliton. Once the soliton has traveled all the way through the crystal, there is a permanent change to the structure.

4.21 Toda Lattice Dynamics

Enrico Fermi (with Pasta & Ulam) was the first person to be seriously concerned with nonlinear coupling in the springs between masses of an array. In Fig. 45 are the time traces of the inner 3 particles of a Toda lattice comprising 5 particles (nonlinear 1-D array). Instead of the normal mode case which the world of physics is familiar with, this system has the capability of soliton like behavior. This system can be made to execute normal mode behavior by operating with a much smaller value of the nonlinearity parameter than the value of 2 used in Fig. 45. For example, try running (GSM program #38) with a value of 0.05. (For information on the Toda lattice, one may refer to Moon's book.)

4.22 Solitons

One topic of considerable importance to the new science of chaos is that of solitary waves, or solitons. The literature concerning this subject tends to be very esoteric; and the language employed is of the type mathematicians, rather than physicists, are familiar with. Almost nothing is mentioned concerning them in introductory textbooks on chaos. A collection of scientific articles, and history, is provided in the book by K. Lonngren and A. Scott, *Solitons in Action*, Academic Press, New York (1978). They describe the 1st observations of solitons by John Scott Russell in the 1830's (water waves on canals

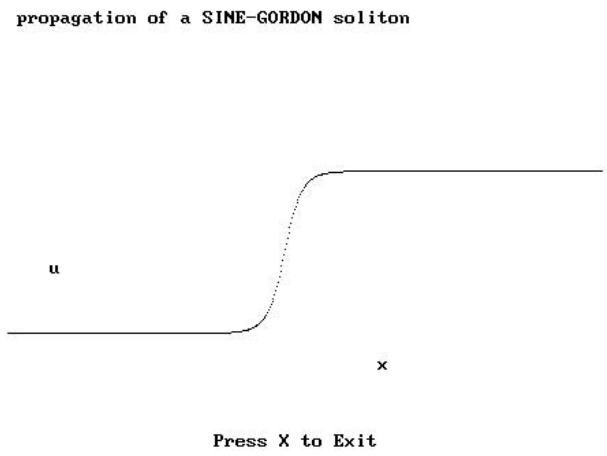

Figure 46: Snapshot of a sine Gordon soliton.

in Britain). Additionally, they note that Fermi, Pasta, and Ulam were the first to use the computer (MANIAC at Los Alamos) to seriously investigate nonlinear differential equations.

4.23 Sine-Gordon equation

The nonlinear partial differential equation which the dislocation kink obeys is given by

$$\partial^2 u/\partial x^2 \; - \; \partial^2 u/\partial t^2 \; = \; sin \; u \tag{34}$$

Detailed information concerning this equation and its various solutions (only one case given here) can be found in E. Enfeld & G. Rowlands, *Nonlinear Waves, Solitons and Chaos*, Cambridge University Press, 1990. In general, the solution can be found in terms of elliptic functions. It can be shown that a special case, single soliton solution is the following

$$\beta \; = \; \sqrt{m^2 - 1}/m \tag{35}$$

$$\xi_1 \; = \; (\underline{+}x - \beta t)/\sqrt{1 - \beta^2} \tag{36}$$

$$\xi_2 \; = \; e^{\xi_1} \quad u \; = \; 4 \, tan^{-1} \xi_2 \tag{37}$$

The "+" sign is the soliton case, and the "-" sign gives the anti-soliton. These are pulse like solutions which are readily studied with GSM program #28. An example execution of this program is provided in Fig. 46, where the soliton is propagating to the right.

4.24 Korteweg deVries equation

Another soliton case is that which is known as KdV. The partial differential equation for this case is (refer to Enfeld and Rowlands, p. 7).

$$\partial u/\partial t \; + \; u \partial u/\partial x \; + \; \partial^3 u/\partial x^3 \; = \; 0 \tag{38}$$

A solution to this equation is the following:

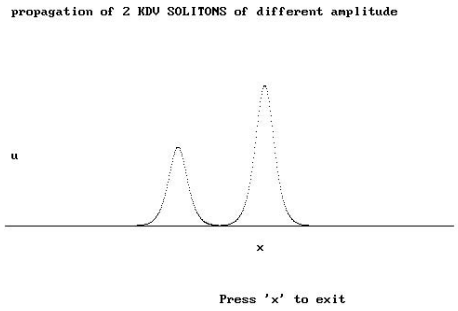

Figure 47: Snapshot of two kdV solitons.

$$\zeta \;=\; \frac{1}{2}a(x - a^2 t) \tag{39}$$

$$u \;=\; 12a^2/(e^{\zeta} + e^{-\zeta})^2 \tag{40}$$

As seen in Fig. 47, from an execution of GSM program #13, this soliton is more nearly the shape of a canal water wave of the type seen by Scott. It also is probably more nearly the type that would be encountered in optical fibers. In Fig. 47 are shown two solitons propagating to the right. The larger of the two moves more rapidly and is leaving the smaller one behind.

5 Krazon

There's a very simple model that holds some promise for treating mesoanelastic complexity. In some respects, it is similar to the Fermi, Pasta, Ulam (FPU) problem. Imagine two particles in a 1-D chain comprising 3 springs, the system held together by two walls. Initially the particles have no displacement, and they are at rest. At t = 0, the walls begin to separate slowly at a constant velocity (adiabatic separation), as illustrated in Fig. 48.

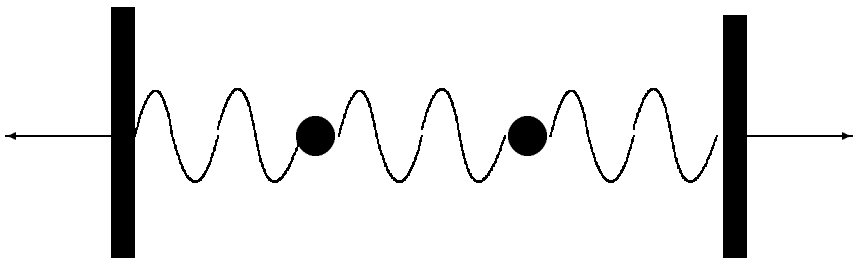

Figure 48: Model of a simple system to generate krazons.

If the springs are Hooke's law springs (harmonic potential), then nothing of interest happens. The particles remain at rest. On the other hand, if the potential between the springs is a cosine modulated parabola (that of the torsion-gravity pendulum shown in Fig. 49), then all kinds of interesting behavior is possible.

The time plot of Fig. 50 was generated with GSM program #14. The particular mode shown is an asymmetric (breathing) mode of the system. Just as with the Toda lattice (nonlinear array based on an exponential function), there are soliton-like and other cooperative phenomena that can exist.

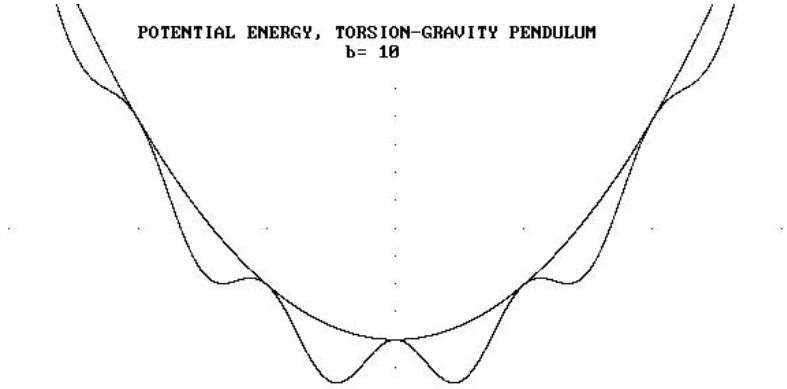

Figure 49: Cosine modulated parabolic potential.

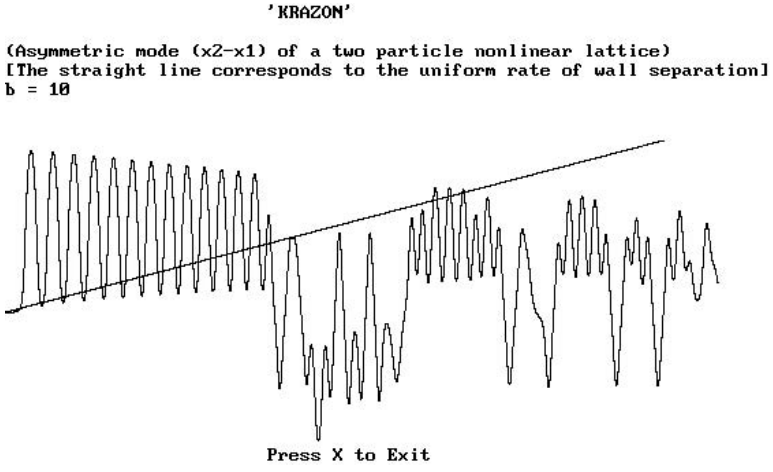

Figure 50: "Krazon" asymmetric mode of a two particle, nonlinear spring system.

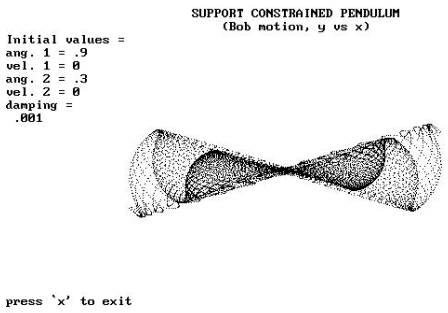

Figure 51: Example trajectory of the support constrained pendulum.

6 Support Constrained Pendulum

The support constrained rigid spherical pendulum is described briefly in part I of this monograph, being illustrated in Fig. 3 (PAPA section 1.5). In dimensionless form, the equations of motion are given by

$$\dot{p_1} \;=\; -\cos q_2 \sin q_1 \;-\; c\, p_1 \tag{41}$$

$$\dot{p_2} \;=\; -\cos q_1 \sin q_2 \;-\; p_1^2 \sin q_2/\cos^3 q_2 \;-\; c\, p_2 \tag{42}$$

$$\dot{q_1} \;=\; p_1/\cos^2 q_2 \tag{43}$$

$$\dot{q_2} \;=\; p_2 \tag{44}$$

The damping terms are the ones multiplied by the dissipation constant, c. In the modeling that was reported in the journal article (Phys. Rev. A 38 (10), 5352 (1988), the damping was different in both axes (and also of a different form than eqns. (41) and (42).

In GSM program #30, the trajectory of the pendulum bob (motion in the x-y plane) is plotted as a function of time. The position at a given time is determined from

$$x \;=\; \sin q_1 \cos q_2 \tag{45}$$

$$y \;=\; \sin q_2 \tag{46}$$

Shown in Fig. 51 is an example output from this routine.

7 Torsion Gravity Pendulum

The torsion gravity pendulum is described in part I of this monograph (section 1.12 of PAPA). Appendix II treats the pendulum in considerable detail. Program numbers 32 through 36 of the General Simulations Menu are all concerned with this pendulum. The reason is that it is easily simulated and also is very versatile.

Only GSM program #36 permits adjustable (large) values of the parameter, b. The others all operate with b = 1.023, corresponding to the system that was experimentally studied and described in the Amer. J. of Physics paper. Sample output from #32 is shown in Fig. 52. The phase space trajectory on the left is a chaotic one, and that on the right is a limit cycle, after transient settling.
It is easy to investigate the power spectra for this pendulum using GSM programs #33 - #35. Chaotic and limit cycle cases for motions similar to those which produced Fig. 52 are illustrated in Fig. 53. The chaotic (left side) case was generated with #35 and #26. The limit cycle (right side) case was generated with #33 and #26. Note the prominent 3rd and 5th harmonics. Program #34 produces a subharmonic response which is rich in spectral content as shown in Fig. 54.

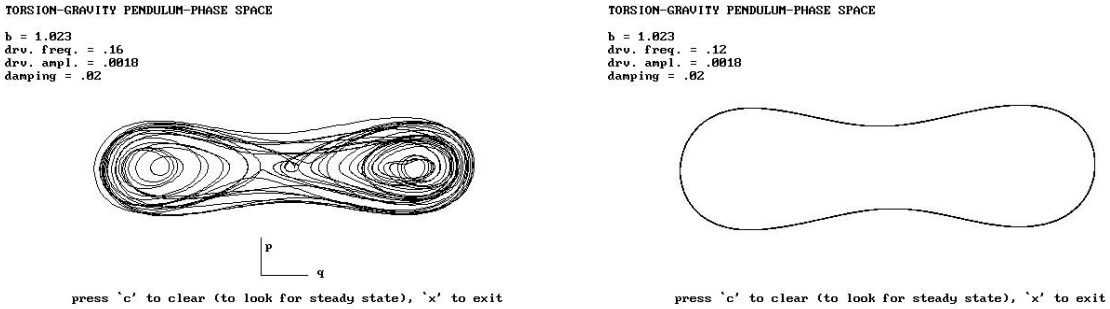

Figure 52: Example Phase Space trajectories of the Torsion Gravity pendulum.

(a). Chaotic case. (b). Period-1 case.

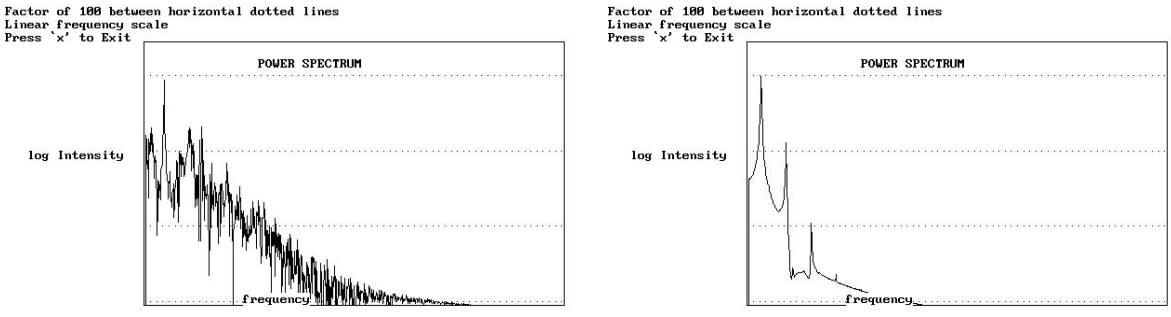

Figure 53: Example Power Spectra associated with Torsion Gravity pendulum motions.

(a). Chaotic case. (b). Period-1 case.

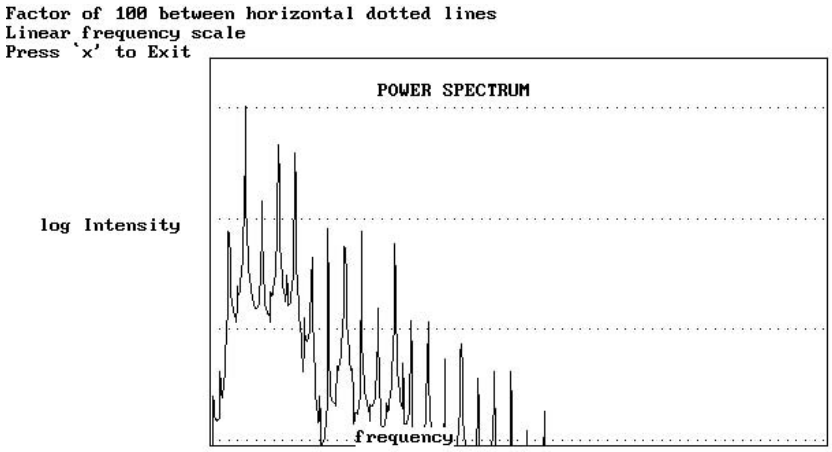

Figure 54: Power spectrum of subharmonic motion, torsion gravity pendulum.

7.1 TGP with large b value

This pendulum is especially interesting when b is large; since among other things, it has strong trapping tendencies. Also, it may be a good candidate for studying boundary chaos. Fig. 55 shows a b=10 case which appears to be initially chaotic; however, after a long time it settles into a period-5 limit cycle. It's not easy to identify the order of the mode in the left side phase space plot; however, the Poincare' section on the right side identifies it immediately. The potential corresponding to this case and also the one of Fig. 56 is pictured in Fig. 49.
With different initial conditions (changing the drive frequency from 0.5 to 0.55), an unusual (chaotic) Poincare' section is realized, as shown in Fig. 56.

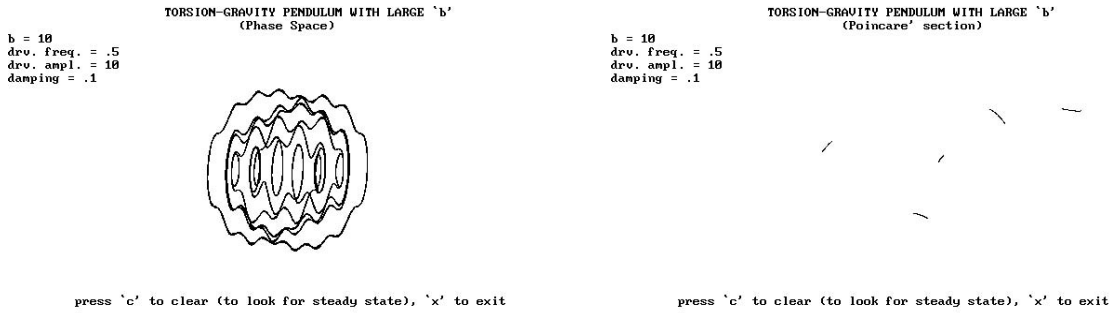

Figure 55: Output from GSM program #34—Torsion gravity pendulum.

(a). Phase Space Trajectory. (b). Poincare' section—period-5 limit cycle of (a) is clearly seen.

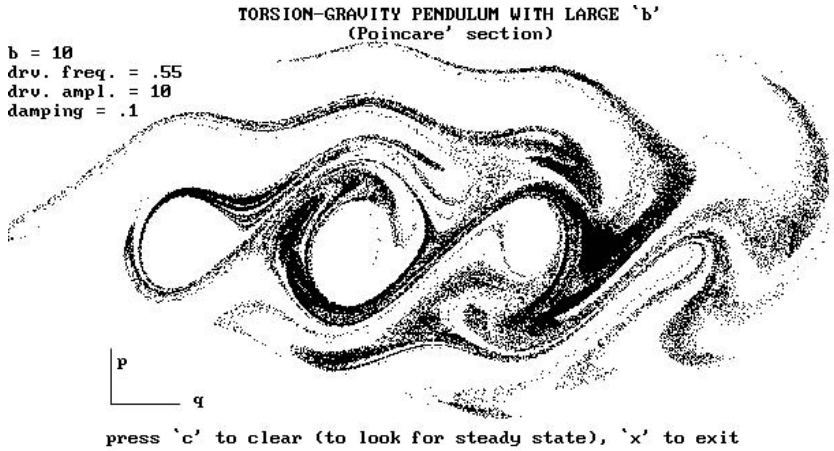

Figure 56: Chaotic Poincare' section, Torsion-Gravity Pendulum with large b.

Index